Technical Memorandum

Date: October 12, 2016

To: PFC 5 Documentation Set

From: David Potyondy

Re: Flat-Joint Contact Model [version 1]

Ref: 5-8106:16TM47

This memo describes the flat-joint contact model (version 1) as provided in the material-modeling support package for the Particle Flow Code (*PFC*, Itasca [2016]).[1] A flat-joint contact and its corresponding flat-jointed material are shown in Figure 8. The flat-joint contact model provides the macroscopic behavior of a finite-size, linear elastic, and either bonded or frictional interface that may sustain partial damage. A flat-jointed material mimics the microstructure of angular, interlocked grains that is similar to marble. The model formulation and test problems are provided in the first and second major sections, respectively. The test problems examine the behaviors of a single flat-jointed contact, and an interlocked grain. The creation and laboratory testing of a flat-jointed material is described in Potyondy (2016, Example Materials 2: Flat-Jointed Material Example).

---

[1] The material-modeling support package (Potyondy, 2016) is provided in the form of a consistent set of FISH functions that operate within *PFC*. FISH is a programming language embedded within PFC. Both *PFC* and the material-modeling support package can be obtained from http://www.itascacg.com/software/pfc. The flat-joint contact model is referred to in commands and FISH by the name **flatjoint**, and its version number is given by the command {**list contact modellist**} and listed in the "Minor" column.

TABLE OF CONTENTS

1.0   FORMULATION

The formulation of the flat-joint contact model is provided in this section. The initial two- and three-dimensional flat-joint models are described in Potyondy (2012a&b) and Potyondy (2013), respectively. The present description defines both the 2D and 3D flat-joint models and supersedes all previous descriptions.

The first three subsections summarize the notational conventions, the PFC model and the kinematic variables — refer to Itasca (2016) and Potyondy (2015) for a complete description of these concepts. The formulation proper begins in the fourth subsection with a description of a flat-joint contact and its corresponding flat-jointed material, and is followed by a description of a flat-jointed interface. The activity-deletion criterion, force-displacement law, energy partitions, properties, methods and call-back events of the flat-joint contact model are then presented, and followed by the stiffnesses required to determine a stable time step. Expressions for element normal force and bending moment that are used in the force-displacement law are provided in the final subsection.

1.1   Notational Conventions

Vectors are denoted by boldface type, such as $\mathbf{v}$. The length or magnitude of $\mathbf{v}$ is denoted $\|\mathbf{v}\|$ or simply v. The addition of a hat denotes a unit vector, such that $\hat{\mathbf{v}} = \mathbf{v}/\|\mathbf{v}\|$. The addition of a dot denotes a time derivative, such as $\dot{\mathbf{v}} = \partial\mathbf{v}/\partial t$. There is a global coordinate system (xyz). The vector $\mathbf{v}$ can be expressed in the global coordinate system by the relations:
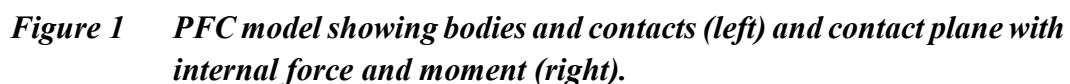
$$\mathbf{v} = \mathbf{v}(x,y,z) = v_x\hat{\mathbf{i}} + v_y\hat{\mathbf{j}} + v_z\hat{\mathbf{k}}$$
$$\text{with } v_x = \mathbf{v}\cdot\hat{\mathbf{i}}, \quad v_y = \mathbf{v}\cdot\hat{\mathbf{j}}, \quad v_z = \mathbf{v}\cdot\hat{\mathbf{k}}$$

(1)

where $\hat{\mathbf{i}}$, $\hat{\mathbf{j}}$ and $\hat{\mathbf{k}}$ are unit vectors directed along the positive x, y and z axes, respectively.

1.2   The PFC Model

The PFC programs (*PFC2D* and *PFC3D*) provide a general purpose, distinct-element modeling framework that includes a computational engine and a graphical user interface. A particular instance of the distinct-element model is referred to as a *PFC model*, which refers to both the 2D and 3D models. The PFC model simulates the movement and interaction of many finite-sized particles. The particles are rigid bodies with finite mass that move independently of one another and can both translate and rotate. Particles interact at pair-wise contacts by means of an internal force and moment. Contact mechanics is embodied in particle-interaction laws that update the internal forces and moments. The time evolution of this system is computed via the distinct-element method, which provides an explicit dynamic solution to Newton's laws of motion. The PFC model provides a

synthetic material consisting of an assembly of rigid grains that interact at contacts and includes both granular and bonded materials.

We here generalize and expand upon the definition of the PFC model given above. The PFC model simulates the movement of particles and their mechanical interaction at pair-wise contacts. We denote each particle as a *body* to clarify that it is not a point mass, but instead, is a rigid body with finite mass and a well-defined surface. The PFC model consists of bodies and *contacts* (see Figure 1). There are three types of bodies: *balls*, *clumps* and *walls*. Bodies have surface properties that are assigned to the *pieces* on the body surface. A ball consists of one piece, which is the ball itself, while the pieces of a clump and wall are called *pebbles* and *facets*, respectively. A ball is a rigid unit-thickness disk in 2D or sphere in 3D. A clump is a collection of pebbles that are rigid unit-thickness disks in 2D or spheres in 3D. Clumps model arbitrarily shaped rigid bodies. The pebbles comprising a clump can overlap but contacts do not exist between them; instead, contacts form between the pebbles on the boundary of a clump and other bodies. A wall is a collection of facets that are linear segments in 2D or triangles in 3D and that form a manifold and orientable surface.

bodies: balls, clumps & walls
balls & pebbles: disks in 2D, spheres in 3D
facets: linear segments in 2D, triangles in 3D

wall (1 piece)

ball (1 piece)

● contact

clump (2 pieces called pebbles)

wall (2 pieces called facets)

$\hat{\mathbf{n}}_c$ $\hat{\mathbf{t}}_c$

n t s $\hat{\mathbf{s}}_c$

$\mathbf{x}_c$

contact plane

interaction volume

$\mathbf{F}_c^{(2)}$

piece 2

piece 1

$\mathbf{F}_c^{(1)}$

$$\mathbf{F}_c^{(1)} = -\mathbf{F}_c, \quad \mathbf{F}_c^{(2)} = \mathbf{F}_c$$
$$\mathbf{M}_c^{(1)} = -\mathbf{M}_c, \quad \mathbf{M}_c^{(2)} = \mathbf{M}_c$$

Internal moments not shown

Figure 1   ***PFC model showing bodies and contacts (left) and contact plane with internal force and moment (right).***

Contact mechanics is embodied in particle-interaction laws that employ a soft-contact approach for which all deformation occurs at the contacts between the rigid bodies. The mechanical interaction between the surfaces of two bodies occurs at one or more pair-wise mechanical contacts. Contacts

are created and deleted based on body proximity by the contact-detection logic. A contact provides an interface between two pieces. The interface consists of a contact plane with location $\left(\mathbf{x}_c \right)$, normal direction $\left(\hat{\mathbf{n}}_c \right)$ and coordinate system $\left(nst \right)$. The contact plane is centered within the interaction volume (either gap or overlap) of the two pieces, oriented tangential to the two pieces and rotated to ensure that relative motion of the piece surfaces remains symmetric w.r.t. the contact plane. Each contact stores a force $\left(\mathbf{F}_c \right)$ and moment $\left(\mathbf{M}_c \right)$ that act at the contact location in an equal and opposite sense on the two pieces. The internal force and moment are updated by the particle-interaction law, which takes the relative motion and surface properties of the two pieces as input. We refer to the particle-interaction law as a *contact model.*

1.3　Kinematic Variables

Kinematics considers the motion of systems of bodies without regard to the role of the forces causing the motion, while kinetics considers the relationship of the forces to the kinematic variables. The kinetics of the PFC model is embodied in the force-displacement law of each contact model. The kinematic variables that serve as the input to the force-displacement law are discussed here — see section "PFC Model Components: Contacts and Contact Models: Contact Resolution" in Itasca (2016) for a more comprehensive discussion.

Contact resolution occurs when a new contact is detected during the cycle sequence, prior to the force-displacement calculations. During contact resolution, the contact state variables (see Table 1) are updated. These variables are defined, and the procedure by which they are computed is described here. Each contact model uses its properties along with the relative motion of the two contacting pieces to update the contact force and moment.

Table 1　Contact State Variables

Property	Description
Contact plane (see Figures 1 and 2)**:**	
$\mathbf{x}_c$	contact-plane location
$\hat{\mathbf{n}}_c$	contact-plane normal direction
$\hat{\mathbf{s}}_c$	contact-plane coord. system (s　axis) (2D model: $\hat{\mathbf{s}}_c \equiv -\hat{\mathbf{k}}$)
$\hat{\mathbf{t}}_c$	contact-plane coord. system (t axis)
g_c	contact gap ($g_c > 0$ is open)
Relative motion (see Figures 5–7)**:**	

$\dot{\boldsymbol{\delta}}$	relative translational velocity
$\dot{\boldsymbol{\theta}}$	relative rotational velocity
$\Delta\delta_n$	relative normal-displacement increment ($\Delta\delta_n > 0$ is opening)
$\Delta\boldsymbol{\delta}_s$	relative shear-displacement increment (2D model: $\Delta\delta_{ss} \equiv 0, \Delta\delta_{st}$)
$\Delta\theta_t$	relative twist-rotation increment (2D model: $\Delta\theta_t \equiv 0$)
$\Delta\boldsymbol{\theta}_b$	relative bend-rotation increment $\left(\Delta\theta_{bs}, \Delta\theta_{bt}\right)$ (2D model: $\Delta\theta_{bk} = -\Delta\theta_{bs}, \Delta\theta_{bt} \equiv 0$)

The contact shown in Figure 2 has been created between the pieces of two bodies. Each contact has two ends, **end1** and **end2**, with the associated pieces and bodies labelled 1 and 2. The bodies are rigid; therefore, the motion of body (b) is described by its rotational velocity $\left(\boldsymbol{\omega}^{(b)}\right)$ and the translational velocity $\left(\dot{\mathbf{x}}^{(b)}\right)$ of its centroid $\left(\mathbf{x}^{(b)}\right)$. The contact state variables include the contact-plane information as well as the contact gap (g_c), which is the minimal signed distance separating the piece surfaces. The kinematic information is described in the next two subsections, which define the contact plane and describe the relative motion of the piece surfaces at a contact. All contact types are described without loss of generality in terms of the two combinations of ball-ball and ball-wall, because balls and pebbles have the same shape.
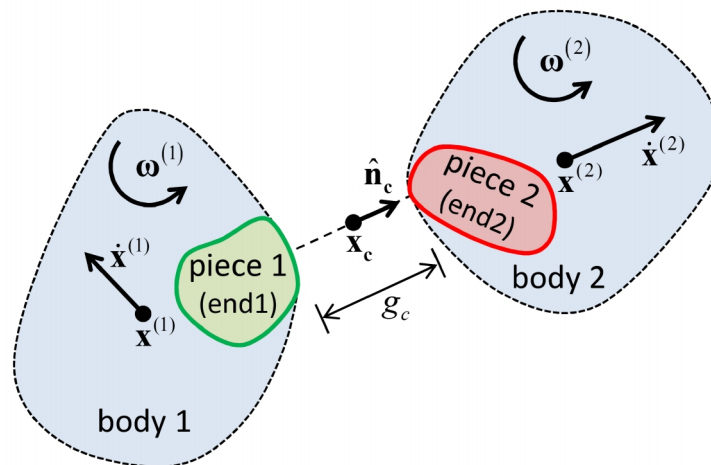

Figure 2   A contact between the pieces of two bodies.

1.3.1 Contact Plane

A contact provides an interface between two pieces (see Figure 5). The interface consists of a contact plane with location ($\mathbf{x_c}$), normal direction ($\hat{\mathbf{n}}_c$) and coordinate system (*nst*).The contact plane is centered within the interaction volume (either gap or overlap) of the two pieces, oriented tangential to the two pieces and rotated to ensure that relative motion of the piece surfaces at the contact location remains symmetric w.r.t. the contact plane.
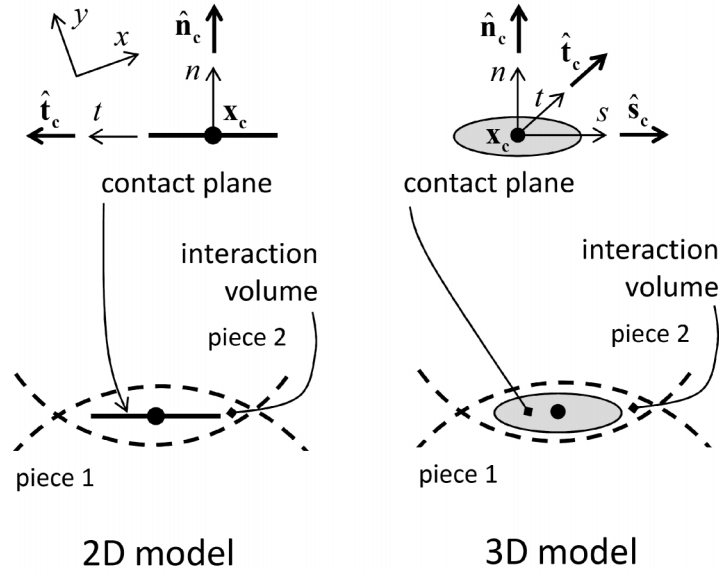

Figure 3 *The contact plane coordinate systems for the 2D and 3D models.*

The contact plane is centered within the interaction volume of the two pieces, directed from piece 1 to piece 2 and oriented tangential to piece 1. The location ($\mathbf{x_c}$) and normal direction ($\hat{\mathbf{n}}_c$) of the contact plane are given by (see Figure 4):

$$\mathbf{x_c} = \mathbf{x}^{(1)} + \left(R^{(1)} + \frac{g_c}{2} \right) \hat{\mathbf{n}}_c, \qquad \hat{\mathbf{n}}_c = \begin{cases} \dfrac{\mathbf{x}^{(2)} - \mathbf{x}^{(1)}}{d}, & \text{ball-ball} \\[2ex] \dfrac{\mathbf{x_f} - \mathbf{x}^{(1)}}{d}, & \text{ball-wall} \end{cases}$$

$$\text{with} \quad g_c = \begin{cases} d - \left(R^{(1)} + R^{(2)} \right), & \text{ball-ball} \\[1ex] d - R^{(1)}, & \text{ball-wall} \end{cases} \tag{2}$$

$$d = \begin{cases} \left\| \mathbf{x}^{(2)} - \mathbf{x}^{(1)} \right\|, & \text{ball-ball} \\[1ex] \left\| \mathbf{x_f} - \mathbf{x}^{(1)} \right\|, & \text{ball-wall} \end{cases}$$

where $\mathbf{x}^{(b)}$ and $R^{(b)}$ are the center and radius, respectively, of ball (b); $\mathbf{x}_f$ is the point on the wall facet that is closest to $\mathbf{x}^{(1)}$; $\mathbf{x}_w$ is the wall center of rotation and g_c is the contact gap. The contact gap is the minimal signed distance separating the piece surfaces such that the gap is negative if the surfaces overlap.
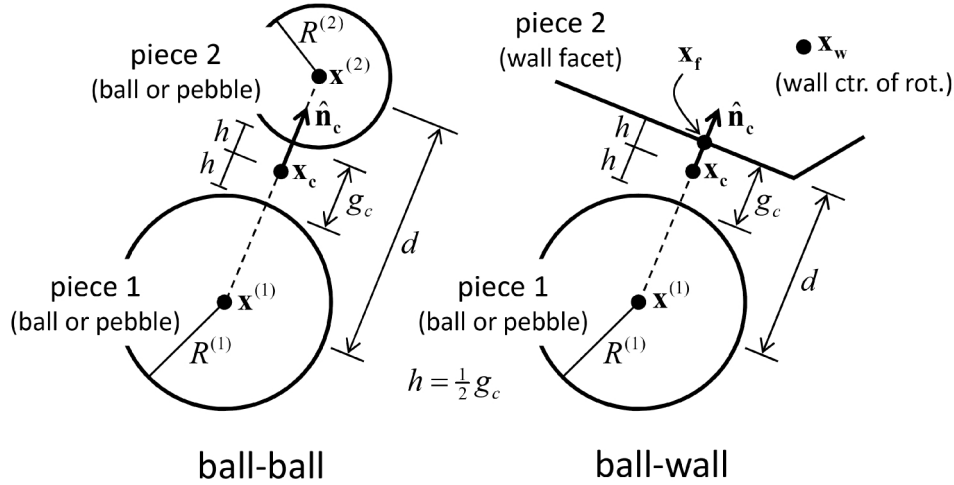

Figure 4 ***The contact plane location and normal direction for the two fundamental contact types: ball-ball and ball-wall.***

The contact plane coordinate system (nst) is oriented such that n coincides with the contact normal direction while s and t are orthogonal coordinates on the plane and $\hat{\mathbf{n}}_c = \hat{\mathbf{s}}_c \times \hat{\mathbf{t}}_c$. The contact plane coordinate system is translated and rotated to ensure that relative motion of the piece surfaces at the contact location remains symmetric w.r.t. the contact plane (as shown in Figures 5 and 6). The translation updates the location and normal direction via Eq. (2). For the 2D model, the following constraints make the rotation implicit:

1. The contact location and normal direction lie in the xy plane such that

$$\mathbf{x}_c = \mathbf{x}_c(x,y,z) = x_{cx}\hat{\mathbf{i}} + x_{cy}\hat{\mathbf{j}} + x_{cz}\hat{\mathbf{k}} \ \left(x_{cz} \equiv 0 \right)$$
$$\hat{\mathbf{n}}_c = \hat{\mathbf{n}}_c(x,y,z) = n_{cx}\hat{\mathbf{i}} + n_{cy}\hat{\mathbf{j}} + n_{cz}\hat{\mathbf{k}} \ \left(n_{cz} \equiv 0 \right).$$

(3)

2. The nt axis lies in the xy plane such that

$$\hat{\mathbf{t}}_c = \hat{\mathbf{k}} \times \hat{\mathbf{n}}_c.$$

(4)

For the 3D model, the s axis is aligned initially with the projection of the global x or y direction, respectively, onto the contact plane (whichever is not parallel with $\hat{\mathbf{n}}_{\mathbf{c}}$), and then the rotation updates the s axis orientation:

$$\hat{\mathbf{s}}_{\mathbf{c}} = \frac{\mathbf{s}_2}{\|\mathbf{s}_2\|}$$

$$\text{with} \quad \mathbf{s}_2 = \mathbf{s}_1 - \mathbf{s}_1 \times \tilde{\boldsymbol{\omega}} \Delta t, \quad \tilde{\boldsymbol{\omega}} = \left(\tfrac{1}{2} \left(\boldsymbol{\omega}^{(1)} + \boldsymbol{\omega}^{(2)} \right) \cdot \hat{\mathbf{n}}_{\mathbf{c}} \right) \hat{\mathbf{n}}_{\mathbf{c}} \tag{5}$$

$$\mathbf{s}_1 = \hat{\mathbf{s}}_{\mathbf{c}}^* - \hat{\mathbf{s}}_{\mathbf{c}}^* \times \left(\hat{\mathbf{n}}_{\mathbf{c}}^* \times \hat{\mathbf{n}}_{\mathbf{c}} \right)$$

where the first rotation (to give $\mathbf{s}_1$) is about the line common to the old and new planes and the second rotation (to give $\mathbf{s}_2$) is about the new normal direction; the star ($*$) denotes the value at the end of the previous time step; $\boldsymbol{\omega}^{(p)}$ is the rotational velocity of piece (p); and $\tilde{\boldsymbol{\omega}}$ is the average rotational velocity of the two pieces about the new normal direction.

A vector quantity that lies on the contact plane ($\mathbf{S}$) can be expressed in the contact plane coordinate system by the relations:

$$\mathbf{S} = \mathbf{S}(s,t) = S_s \hat{\mathbf{s}}_{\mathbf{c}} + S_t \hat{\mathbf{t}}_{\mathbf{c}} \quad (\text{2D model: } S_s \equiv 0)$$

$$\text{with} \quad S_s = \mathbf{S} \cdot \hat{\mathbf{s}}_{\mathbf{c}}, \quad S_t = \mathbf{S} \cdot \hat{\mathbf{t}}_{\mathbf{c}}. \tag{6}$$

1.3.2   Relative Motion at a Contact

The relative motion of the piece surfaces at a contact is described by the relative translational $\left(\dot{\boldsymbol{\delta}} \right)$ and rotational $\left(\dot{\boldsymbol{\theta}} \right)$ velocities:

$$\dot{\boldsymbol{\delta}} = \dot{\mathbf{x}}_{\mathbf{c}}^{(2)} - \dot{\mathbf{x}}_{\mathbf{c}}^{(1)}$$

$$\dot{\boldsymbol{\theta}} = \boldsymbol{\omega}^{(2)} - \boldsymbol{\omega}^{(1)}. \tag{7}$$

In this expression, $\dot{\mathbf{x}}_{\mathbf{c}}^{(b)}$ is the translational velocity of body (b) at the contact location:

$$\dot{\mathbf{x}}_{\mathbf{c}}^{(b)} = \dot{\mathbf{x}}^{(b)} + \boldsymbol{\omega}^{(b)} \times \left(\mathbf{x}_{\mathbf{c}} - \mathbf{x}^{(b)} \right) \tag{8}$$

where $\dot{\mathbf{x}}^{(b)}$ is the translational velocity at the centroid of body (b); $\boldsymbol{\omega}^{(b)}$ is the rotational velocity of body (b); $\mathbf{x}_{\mathbf{c}}$ is the contact location and $\mathbf{x}^{(b)}$ is either the centroid (if the body is a ball or clump) or

the center of rotation (if the body is a wall) of body (b). The contact location defines a point that is fixed w.r.t. each body, and thus, $\dot{\mathbf{x}}_{\mathbf{c}}^{(b)}$ is the translational velocity of that point in body (b).[2]

The relative translational velocity can be expressed as

$$
\begin{aligned}
&\dot{\boldsymbol{\delta}} = \dot{\boldsymbol{\delta}}_{\mathbf{n}} + \dot{\boldsymbol{\delta}}_{\mathbf{s}} \\
&\text{with} \quad \dot{\boldsymbol{\delta}}_{\mathbf{n}} = \left(\dot{\boldsymbol{\delta}} \cdot \hat{\mathbf{n}}_{\mathbf{c}} \right) \hat{\mathbf{n}}_{\mathbf{c}} = \dot{\delta}_n \hat{\mathbf{n}}_{\mathbf{c}}, \quad \dot{\boldsymbol{\delta}}_{\mathbf{s}} = \dot{\boldsymbol{\delta}} - \dot{\boldsymbol{\delta}}_{\mathbf{n}}
\end{aligned}
\tag{9}
$$

where $\dot{\boldsymbol{\delta}}_{\mathbf{n}}$ ($\dot{\delta}_n > 0$ is moving apart) and $\dot{\boldsymbol{\delta}}_{\mathbf{s}}$ are the relative translational velocities normal and tangential, respectively, to the contact plane, and the subscripts n and s correspond with normal and shear action, respectively (see Figures 5 and 7 — the centering of the contact within the interaction volume ensures that the relative displacement is symmetric w.r.t. the contact plane). For the 2D model, Eq. (9) satisfies the condition: $\dot{\delta}_{ss} \equiv 0$.

The relative rotational velocity can be expressed as

$$
\begin{aligned}
&\dot{\boldsymbol{\theta}} = \dot{\boldsymbol{\theta}}_{\mathbf{t}} + \dot{\boldsymbol{\theta}}_{\mathbf{b}} \\
&\text{with} \quad \dot{\boldsymbol{\theta}}_{\mathbf{t}} = \left(\dot{\boldsymbol{\theta}} \cdot \hat{\mathbf{n}}_{\mathbf{c}} \right) \hat{\mathbf{n}}_{\mathbf{c}} = \dot{\theta}_t \hat{\mathbf{n}}_{\mathbf{c}}, \quad \dot{\boldsymbol{\theta}}_{\mathbf{b}} = \dot{\boldsymbol{\theta}} - \dot{\boldsymbol{\theta}}_{\mathbf{t}}
\end{aligned}
\tag{10}
$$

where $\dot{\boldsymbol{\theta}}_{\mathbf{t}}$ ($\dot{\theta}_t > 0$ is shown in Figure 6) and $\dot{\boldsymbol{\theta}}_{\mathbf{b}}$ are the relative rotational velocities normal and tangential, respectively, to the contact plane, and the subscripts t and b correspond with twisting and bending action, respectively (see Figures 6 and 7). For the 2D model, Eq. (10) satisfies the conditions: $\dot{\boldsymbol{\theta}}_{\mathbf{t}} \equiv \mathbf{0}$ and $\dot{\boldsymbol{\theta}}_{\mathbf{b}}$ is aligned with the z axis such that $\dot{\theta}_{bt} \equiv 0$ and $\dot{\theta}_{bk} = -\dot{\theta}_{bs}$.

The relative displacement and rotation increments at the contact during a time step Δt are

$$
\begin{aligned}
&\Delta \boldsymbol{\delta} = \Delta \delta_n \hat{\mathbf{n}}_{\mathbf{c}} + \Delta \boldsymbol{\delta}_{\mathbf{s}} \left[\Delta \delta_{ss} = \Delta \boldsymbol{\delta}_{\mathbf{s}} \cdot \hat{\mathbf{s}}_{\mathbf{c}}, \ \Delta \delta_{st} = \Delta \boldsymbol{\delta}_{\mathbf{s}} \cdot \hat{\mathbf{t}}_{\mathbf{c}} \right] \\
&\Delta \boldsymbol{\theta} = \Delta \theta_t \hat{\mathbf{n}}_{\mathbf{c}} + \Delta \boldsymbol{\theta}_{\mathbf{b}} \left[\Delta \theta_{bs} = \Delta \boldsymbol{\theta}_{\mathbf{b}} \cdot \hat{\mathbf{s}}_{\mathbf{c}}, \ \Delta \theta_{bt} = \Delta \boldsymbol{\theta}_{\mathbf{b}} \cdot \hat{\mathbf{t}}_{\mathbf{c}} \right] \\
&\text{with} \quad \Delta \delta_n = \dot{\delta}_n \Delta t, \quad \Delta \boldsymbol{\delta}_{\mathbf{s}} = \dot{\boldsymbol{\delta}}_{\mathbf{s}} \Delta t \\
&\qquad\quad \Delta \theta_t = \dot{\theta}_t \Delta t, \quad \Delta \boldsymbol{\theta}_{\mathbf{b}} = \dot{\boldsymbol{\theta}}_{\mathbf{b}} \Delta t
\end{aligned}
\tag{11}
$$

---

[2] The location of this point within each body may change — e.g., under increasing applied compression, the overlap increases and these points move deeper into each body.

where $\Delta\delta_n$ is the relative normal-displacement increment, $\Delta\boldsymbol{\delta}_s$ is the relative shear-displacement increment, $\Delta\theta_t$ is the relative twist-rotation increment and $\Delta\boldsymbol{\theta}_b$ is the relative bend-rotation increment. For the 2D model, Eq. (11) satisfies the conditions: $\Delta\delta_{ss} \equiv \Delta\theta_t \equiv \Delta\theta_{bt} \equiv 0$ and $\Delta\theta_{bk} = -\Delta\theta_{bs}$.
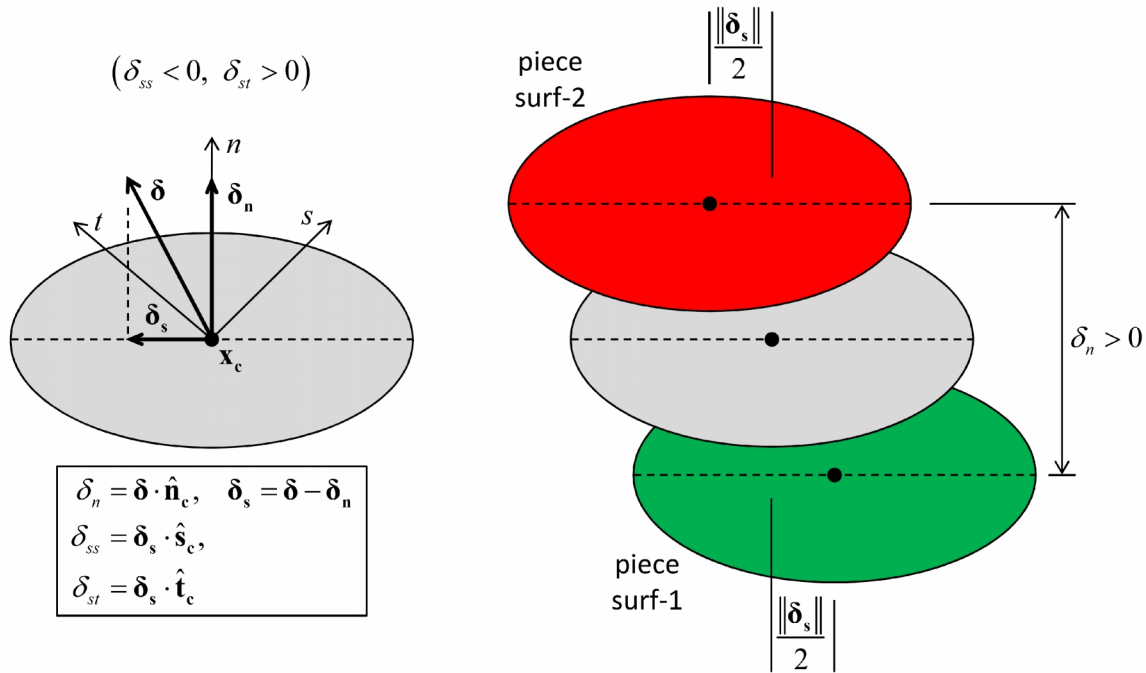

$$\delta_n = \boldsymbol{\delta}\cdot\hat{\mathbf{n}}_\mathbf{c}, \quad \boldsymbol{\delta}_\mathbf{s} = \boldsymbol{\delta}-\boldsymbol{\delta}_\mathbf{n}$$
$$\delta_{ss} = \boldsymbol{\delta}_\mathbf{s}\cdot\hat{\mathbf{s}}_\mathbf{c},$$
$$\delta_{st} = \boldsymbol{\delta}_\mathbf{s}\cdot\hat{\mathbf{t}}_\mathbf{c}$$

Figure 5　　**Kinematics of a contact showing contact plane with relative displacement and motion of piece surfaces.**
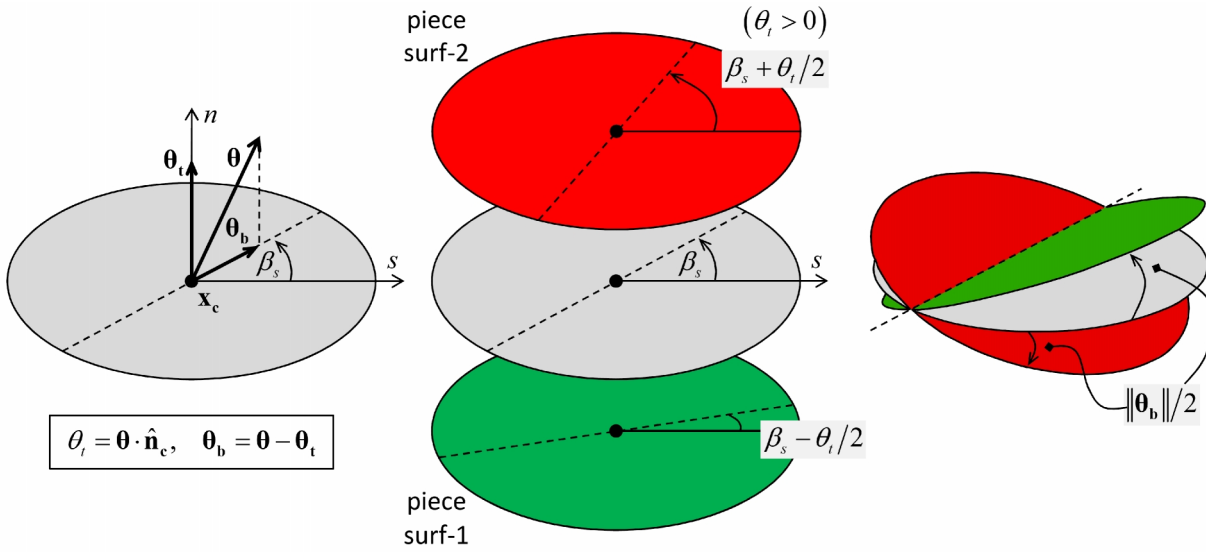
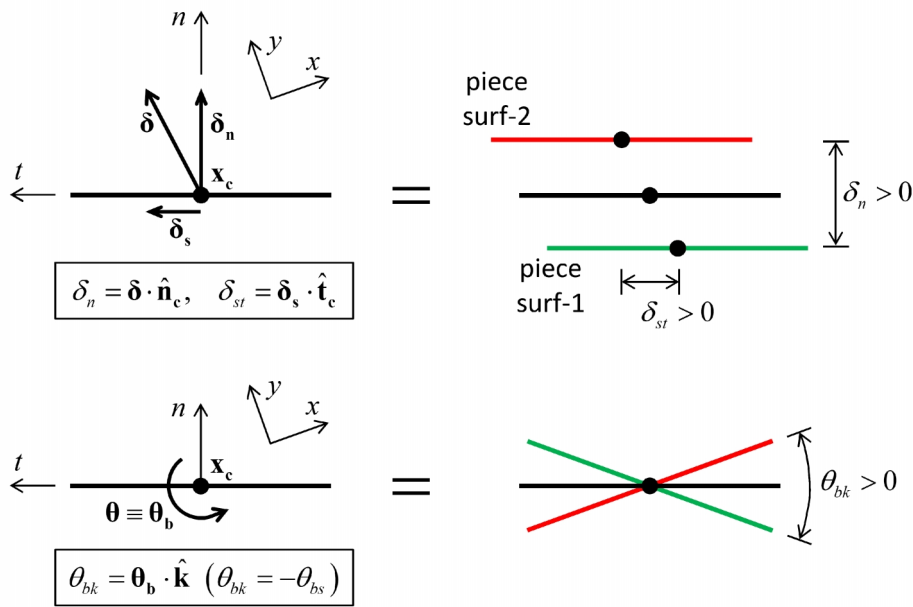**Figure 6** *Kinematics of a contact showing contact plane with relative rotation and motion of piece surfaces.*

Figure 7 *Kinematics of a contact for the 2D model showing contact plane with relative displacement and rotation and motion of piece surfaces.*

1.4 Flat-Jointed Material

A flat-joint contact and its corresponding flat-jointed material are shown in Figure 8. The flat-joint contact model provides the macroscopic behavior of a finite-size, linear elastic, and either bonded or frictional interface that may sustain partial damage. A flat-jointed material is defined in Potyondy (2016) as a granular assembly in which the flat-joint contact model exists at all grain-grain contacts with a gap less than or equal to the installation gap at the end of the material-finalization phase; all

other grain-grain contacts as well as new grain-grain contacts that may form during subsequent motion are assigned the linear contact model. A flat-jointed material mimics the microstructure of angular, interlocked grains that is similar to marble.
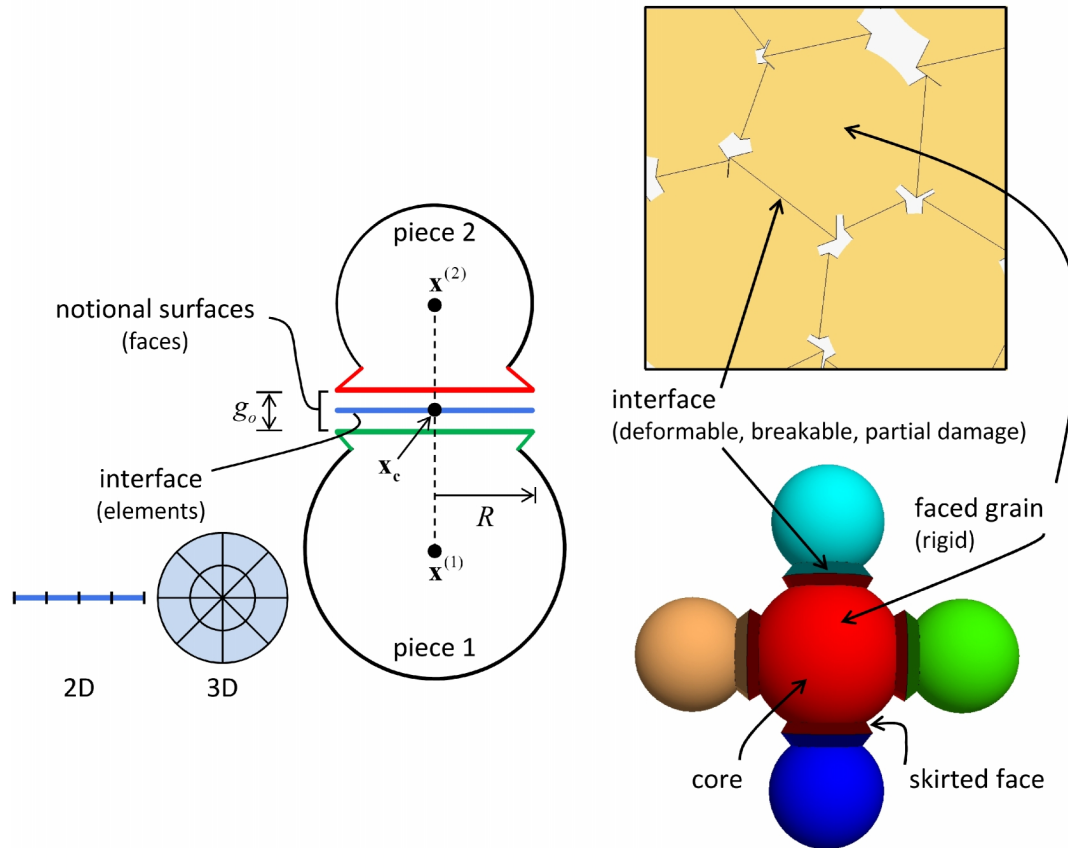

Figure 8   ***Flat-joint contact (left) and flat-jointed material (right).***

The flat-joint contact model provides the macroscopic behavior of a finite-size, linear elastic and either bonded or frictional interface that may sustain partial damage (see Figure 9). The interface is discretized into elements. Each element is either bonded or unbonded, and the breakage of each bonded element contributes partial damage to the interface. The behavior of a bonded element is linear elastic until the strength limit is exceeded and the bond breaks making the element unbonded, while the behavior of an unbonded element is linear elastic and frictional with slip accommodated by imposing a Coulomb limit on the shear force. Each element carries a force and moment that obey the force-displacement law described below, while the force-displacement response of the flat-joint interface is an emergent behavior that includes evolving from a fully bonded state to a fully unbonded and frictional state.
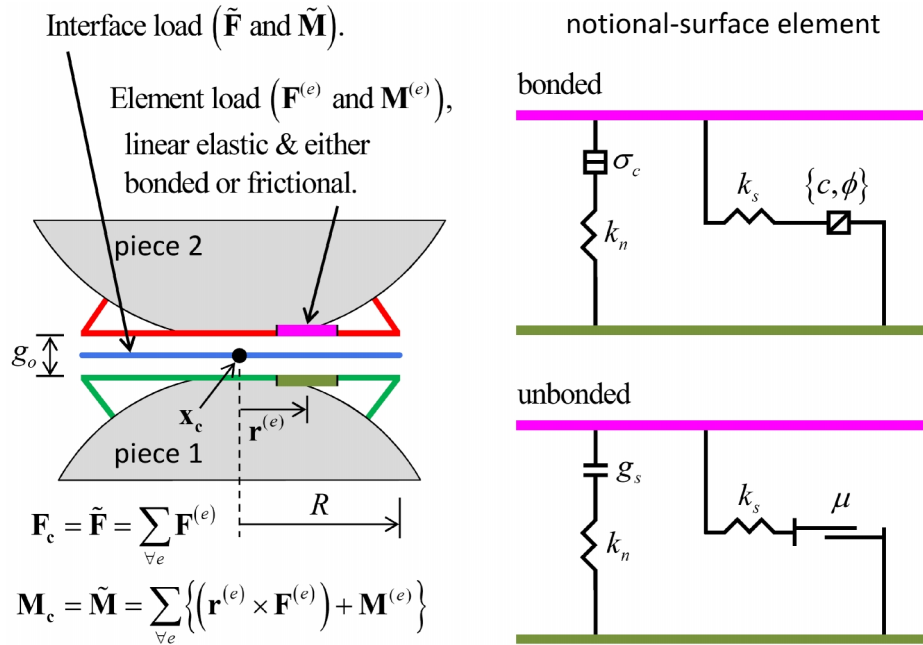
Interface load $\left(\tilde{\mathbf{F}} \text{ and } \tilde{\mathbf{M}}\right)$.

notional-surface element

Element load $\left(\mathbf{F}^{(e)} \text{ and } \mathbf{M}^{(e)}\right)$, linear elastic & either bonded or frictional.

piece 2

piece 1

$$\mathbf{F_c} = \tilde{\mathbf{F}} = \sum_{\forall e} \mathbf{F}^{(e)}$$

$$\mathbf{M_c} = \tilde{\mathbf{M}} = \sum_{\forall e}\left\{\left(\mathbf{r}^{(e)} \times \mathbf{F}^{(e)}\right) + \mathbf{M}^{(e)}\right\}$$

Figure 9   *Behavior and rheological components of the flat-joint model.*

A flat-joint contact simulates the behavior of an interface between two notional surfaces, each of which is connected rigidly to a piece of a body. A flat-jointed material consists of bodies (balls, clumps or walls) joined by flat-joint contacts such that the effective surface of each body is defined by the notional surfaces of its pieces, which interact at each flat-joint contact with the notional surface of the contacting piece. The notional surfaces are called faces, which are lines in 2D and disks in 3D.

The following description of a flat-jointed material applies to the case in which bodies are balls; however, the flat-joint model can be installed at both ball-ball and ball-wall contacts. We refer to the balls of a flat-jointed material as faced grains, each of which is depicted as a circular or spherical core and a number of skirted faces. The faced grains are created when the flat-joint model is installed at the ball-ball contacts of a packed ball assembly (see Figure 10). An interface exists between each set of adjoining faces and is discretized into elements with each element being either bonded or unbonded. The breakage of each bonded element contributes partial damage to the interface, and each breakage event is denoted as a crack (see Figure 11).[3] If the relative displacement at a flat-joint contact becomes larger than the flat-joint diameter, then the adjoining faces may be removed (because the contact may be deleted) making the associated balls locally circular or spherical; if

---

[3] A crack is a disk for the 3D model and a linear segment of unit-thickness depth for the 2D model. A crack has failure mode (tensile or shear) and geometric information (size, position, normal direction and gap). The size is two times the element radius (which is the radius giving the same area as the element), or the element length for the 2D model. The position, normal direction and gap are updated to correspond with material motion subsequent to bond breakage. Cracks are displayed by the crack-monitoring package (see section "Crack Monitoring" in Potyondy [2016]).

these balls come back into contact, the behavior will be that of an interface between circular or spherical surfaces (if the linear contact model is assigned to the new contact).
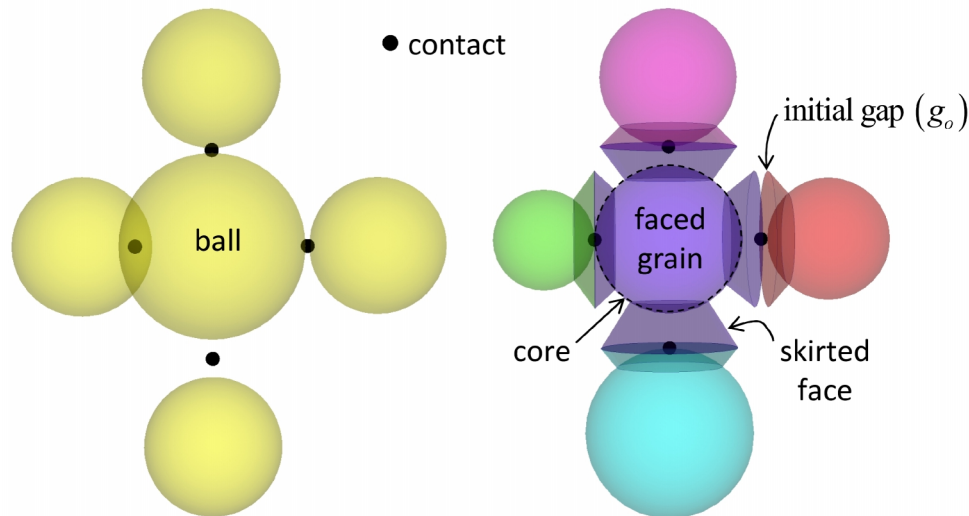

Figure 10 *Creation of faced grains showing packed ball assembly (left) and initial faced-grain assembly (right).*
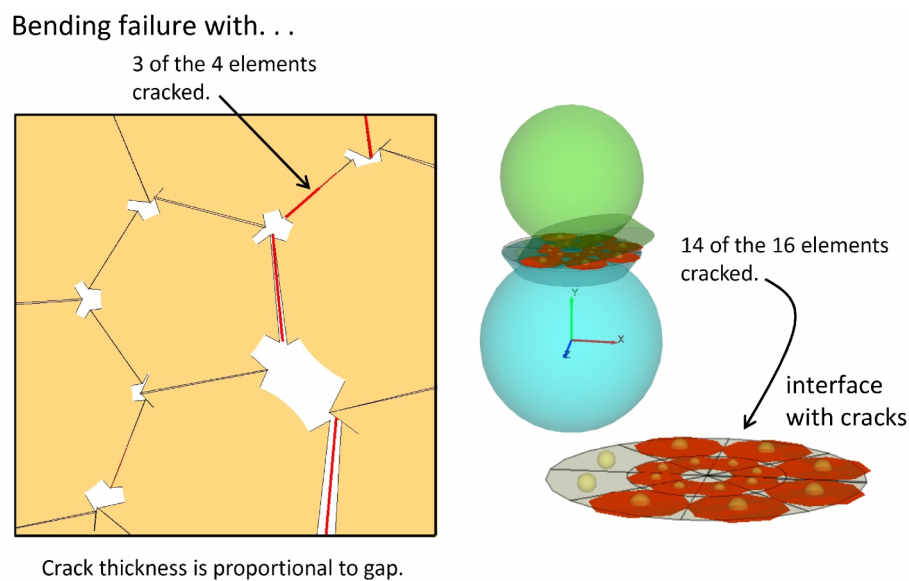

Figure 11 *Partially damaged flat-jointed material showing faced grains with cracks colored red/blue for tensile/shear failure.*

1.5 Flat-Jointed Interface

The interface of the flat-joint model remains centered on, and rotates with, the contact plane such that the interface coordinate system coincides with the contact-plane coordinate system. The interface gap $(g, g > 0$ is open$)$ is expressed below in terms of the surface gap and the relative

bend-rotation vector.[4] The relative motion of the notional surfaces varies over the interface and is expressed by the symbols $\widehat{\delta}$ and $\widehat{\theta}$, which are related to the relative motion of the piece surfaces at the contact location:

$$
\begin{aligned}
\Delta\widehat{\boldsymbol{\delta}} &= \Delta\delta_n\hat{\mathbf{n}}_{\mathbf{c}} + \Delta\widehat{\boldsymbol{\delta}}_{\mathbf{s}} \\
\Delta\widehat{\boldsymbol{\theta}} &\equiv \Delta\boldsymbol{\theta} \\
\text{with}\quad \Delta\widehat{\boldsymbol{\delta}}_{\mathbf{s}} &= \Delta\boldsymbol{\delta}_{\mathbf{s}} + \left(\Delta\boldsymbol{\theta}_{\mathbf{t}}\times\mathbf{r}\right) = \dot{\boldsymbol{\delta}}_{\mathbf{s}}\Delta t + \left(\dot{\boldsymbol{\theta}}_{\mathbf{t}}\Delta t\times\mathbf{r}\right) \\
&\left[\Delta\widehat{\delta}_{ss} = \Delta\widehat{\boldsymbol{\delta}}_{\mathbf{s}}\cdot\hat{\mathbf{s}}_{\mathbf{c}}, \;\; \Delta\widehat{\delta}_{st} = \Delta\widehat{\boldsymbol{\delta}}_{\mathbf{s}}\cdot\hat{\mathbf{t}}_{\mathbf{c}}\right]
\end{aligned}
\tag{12}
$$

where the relative displacement and rotation increments ($\Delta\boldsymbol{\delta}$ and $\Delta\boldsymbol{\theta}$) are from Eq. (11). It is only the relative shear displacement ($\Delta\widehat{\boldsymbol{\delta}}_{\mathbf{s}}$) of the 3D model that varies over the interface (when the relative twist rotation is non-zero); thus, the circumflex will be used only for this quantity. In the remainder of this section, we describe the kinematic variables and interface discretization, first for the 2D model and then for the 3D model.

The interface of the 2D flat-joint model is a rectangle of width $2R$ and unit-thickness depth. The location of a point $\mathbf{x}$ that lies on the interface is expressed by its relative position $\mathbf{r}=\mathbf{x}-\mathbf{x}_{\mathbf{c}}$. The interface discretization (see Figure 12) is controlled by the number of equal-length elements in the radial direction (N_r). The area and centroid location of each element are denoted by $A^{(e)}$ and $\mathbf{x}^{(e)}$, respectively. These quantities are given by

$$
\begin{aligned}
A^{(e)} &= \frac{2Rt}{N_r} \;\; (t=1) \\
\mathbf{x}^{(e)} &= \mathbf{x}_{\mathbf{c}} + \mathbf{r}^{(e)}, \quad e=1,2,\ldots,N_r \\
\text{with}\quad \mathbf{r}^{(e)} &= \rho^{(e)}\hat{\mathbf{t}}_{\mathbf{c}} \\
\rho^{(e)} &= R\left(\frac{-2e+1+N_r}{N_r}\right).
\end{aligned}
\tag{13}
$$

The quantities $A^{(e)}$ and $\rho^{(e)}$ do not change during a simulation; thus, they are set and stored during the first cycle after flat-joint installation.

---

[4] The kinematic formulation approximates the motion of two notional surfaces, each of which is connected rigidly to a piece of a body. A limitation of the current formulation is that when two bodies joined by a flat-joint contact are moved tangentially to one another, the interface gap increases (because g_s increases). It may be possible to remove this limitation by introducing an alternative interface coordinate system that does not rotate under the above condition.
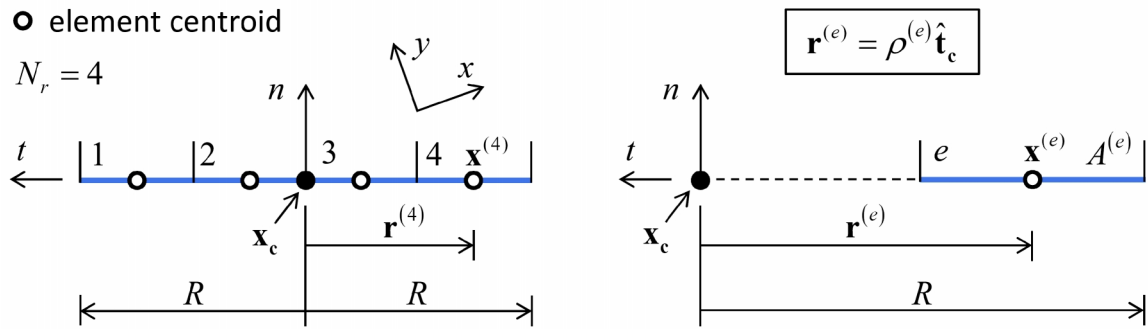
Figure 12 *Interface discretization of the 2D flat-joint model showing element-numbering convention (left) and parameterization of a typical element (right).*

The interface gap of the 2D flat-joint model (see Figure 13) is given by

$$g(\mathbf{r}) = g(\gamma) = g_s + (\gamma - R)\theta_{bk} \quad (\text{small-angle approx. } \theta_{bk} \cong \tan\theta_{bk})$$
$$\text{with} \quad \theta_{bk} = \mathbf{\theta_b} \cdot \hat{\mathbf{k}}, \quad \gamma \in [0, 2R] \tag{14}$$

where g_s is the surface gap and $\mathbf{\theta_b}$ is the relative bend-rotation vector of Eq. (11). When expressed in the γ system, the interface gap varies only with γ and is related to g_s and θ_{bk} — the interface gap is not affected by the relative shear motion (which is a small-strain approximation).
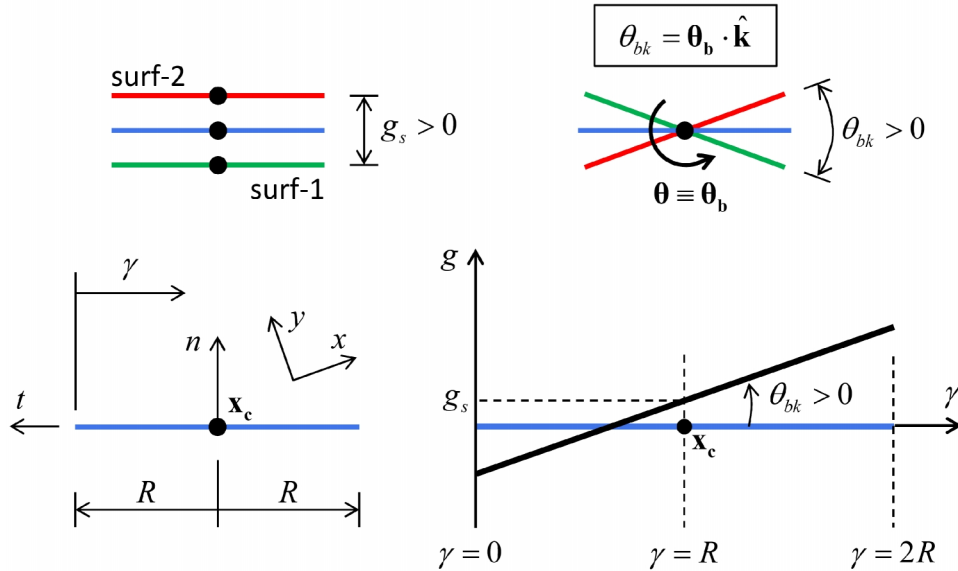

Figure 13 *Interface gap of the 2D flat-joint model corresponding with motion at top of image.*

For the 2D flat-joint model, the following components of the interface relative motion are tracked:

$$
\begin{aligned}
g_s &:= g_s + \Delta \delta_n \\
\delta_{st} &:= \delta_{st} + \Delta \boldsymbol{\delta_s} \cdot \hat{\mathbf{t}}_{\mathbf{c}} \\
\theta_{bk} &:= \theta_{bk} + \Delta \boldsymbol{\theta_b} \cdot \hat{\mathbf{k}}.
\end{aligned}
\tag{15}
$$

The interface of the 3D flat-joint model is a disk of diameter $2R$. The location of a point $\mathbf{x}$ that lies on the interface is expressed by its relative position $\mathbf{r} = \mathbf{x} - \mathbf{x_c}$. The interface discretization (see Figure 14) is controlled by the number of elements in the radial (N_r) and circumferential (N_α) directions. The area and centroid location of each element are denoted by $A^{(e)}$ and $\mathbf{x}^{(e)}$, respectively. These quantities are given by

$$
\begin{aligned}
A^{(e)} &= \int dA = \frac{1}{2} \left(\alpha_2 - \alpha_1 \right) \left(r_2^2 - r_1^2 \right), \quad r_1 < r_2, \quad \alpha_1 < \alpha_2, \quad e = 1, 2, \ldots, N_r N_\alpha \\
\mathbf{x}^{(e)} &= \mathbf{x_c} + \mathbf{r}^{(e)} \\
\text{with} \quad \mathbf{r}^{(e)} &= r_s^{(e)} \hat{\mathbf{s}}_{\mathbf{c}} + r_t^{(e)} \hat{\mathbf{t}}_{\mathbf{c}} = s^{(e)} \hat{\mathbf{s}}_{\mathbf{c}} + t^{(e)} \hat{\mathbf{t}}_{\mathbf{c}} \\
s^{(e)} &= \frac{\int s\, dA}{\int dA} = \frac{2}{3} \left(\frac{\sin \alpha_2 - \sin \alpha_1}{\alpha_2 - \alpha_1} \right) \left(\frac{r_2^3 - r_1^3}{r_2^2 - r_1^2} \right) \\
t^{(e)} &= \frac{\int t\, dA}{\int dA} = \frac{2}{3} \left(\frac{\cos \alpha_1 - \cos \alpha_2}{\alpha_2 - \alpha_1} \right) \left(\frac{r_2^3 - r_1^3}{r_2^2 - r_1^2} \right)
\end{aligned}
\tag{16}
$$

where the superscript-(e) notation has been dropped for the r and α terms, which are given by

$$
\begin{aligned}
r_1^{(e)} &= I \Delta r, \quad e = 1, 2, \ldots, N_r N_\alpha \\
r_2^{(e)} &= (I + 1) \Delta r \\
\alpha_1^{(e)} &= J \Delta \alpha \\
\alpha_2^{(e)} &= (J + 1) \Delta \alpha \\
\text{with} \quad \Delta r &= R / N_r, \quad \Delta \alpha = 2\pi / N_\alpha \\
I &= \left\lfloor (e-1) / N_\alpha \right\rfloor, \quad J = e - 1 - I N_\alpha
\end{aligned}
\tag{17}
$$

where $\text{floor}(x) = \lfloor x \rfloor$ is the largest integer not greater than x. The quantities $A^{(e)}$, $s^{(e)}$ and $t^{(e)}$ do not change during a simulation; thus, they are set and stored during the first cycle after flat-joint installation.

○ element centroid

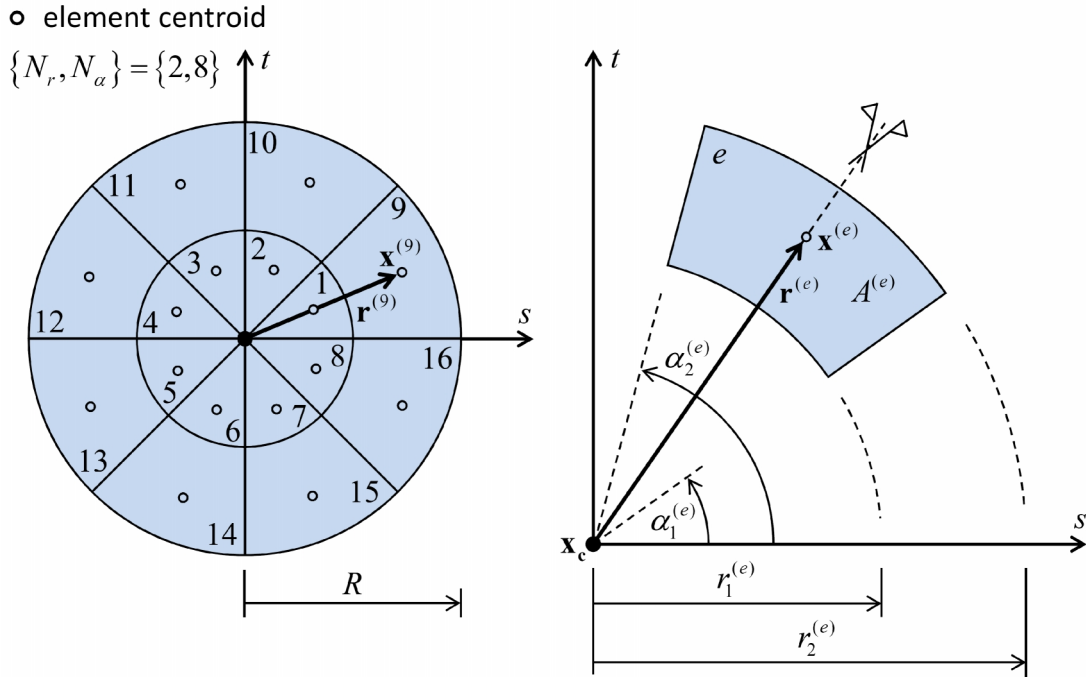$\{N_r, N_\alpha\} = \{2,8\}$

Figure 14   Interface discretization of the 3D flat-joint model showing element-numbering convention (left) and parameterization of a typical element (right).

There are two coordinate systems associated with the interface of the 3D flat-joint model (see Figure 15): the *nst* system, which coincides with the contact plane coordinate system and the *nξη* system, which is dependent on the contact plane coordinate system as follows. The relative bend-rotation vector ($\mathbf{\theta_b}$) orients the *nξη* coordinate system such that ξ is aligned with $\mathbf{\theta_b}$ (at an angle β_s from the positive s axis) and $\hat{\mathbf{n}}_c = \hat{\mathbf{\xi}} \times \hat{\mathbf{\eta}}$. The relative position of a point $\mathbf{x}$ that lies on the interface can be expressed in either coordinate system by the relations:

$$\begin{aligned}
\mathbf{r} &= \mathbf{x} - \mathbf{x_c} \\
&= \mathbf{r}(s,t) = r_s \hat{\mathbf{s}}_c + r_t \hat{\mathbf{t}}_c \\
&= \mathbf{r}(\xi,\eta) = r_\xi \hat{\mathbf{\xi}} + r_\eta \hat{\mathbf{\eta}}
\end{aligned}$$

(18)

$$\text{with}\quad r_s = \mathbf{r} \cdot \hat{\mathbf{s}}_c = s, \quad r_t = \mathbf{r} \cdot \hat{\mathbf{t}}_c = t$$
$$r_\xi = \mathbf{r} \cdot \hat{\mathbf{\xi}} = \xi, \quad r_\eta = \mathbf{r} \cdot \hat{\mathbf{\eta}} = \eta.$$

The mapping between these two coordinate systems of a vector $\mathbf{S}$ that lies on the interface is given by the relations:

$$\begin{Bmatrix} S_\xi \\ S_\eta \end{Bmatrix} = \begin{bmatrix} \mathbf{t_{gl}} \end{bmatrix} \begin{Bmatrix} S_s \\ S_t \end{Bmatrix}, \quad \begin{Bmatrix} S_s \\ S_t \end{Bmatrix} = \begin{bmatrix} \mathbf{t_{gl}} \end{bmatrix}^T \begin{Bmatrix} S_\xi \\ S_\eta \end{Bmatrix}$$

$$\begin{bmatrix} \mathbf{t_{gl}} \end{bmatrix} = \begin{bmatrix} \cos\beta_s & \sin\beta_s \\ -\sin\beta_s & \cos\beta_s \end{bmatrix} \tag{19}$$

$$\xi_s = \hat{\boldsymbol{\xi}} \cdot \hat{\mathbf{s}}_\mathbf{c} = \cos\beta_s, \quad \xi_t = \hat{\boldsymbol{\xi}} \cdot \hat{\mathbf{t}}_\mathbf{c} = \sin\beta_s$$

$$\eta_s = \hat{\boldsymbol{\eta}} \cdot \hat{\mathbf{s}}_\mathbf{c} = -\sin\beta_s, \quad \eta_t = \hat{\boldsymbol{\eta}} \cdot \hat{\mathbf{t}}_\mathbf{c} = \cos\beta_s.$$

The interface gap of the 3D flat-joint model (see Figure 15) is given by

$$g(\mathbf{r}) = g(\xi, \eta) = g_s + \eta\theta_{b\xi} \quad \left(\text{small-angle approx. } \theta_{b\xi} \cong \tan\theta_{b\xi}\right)$$

$$\text{with} \quad \theta_{b\xi} = \boldsymbol{\theta}_\mathbf{b} \cdot \hat{\boldsymbol{\xi}} = \|\boldsymbol{\theta}_\mathbf{b}\|, \quad \{\xi, \eta\} \in [-R, R] \tag{20}$$

where g_s is the surface gap and $\boldsymbol{\theta}_\mathbf{b}$ is the relative bend-rotation vector of Eq. (11). When expressed in the $n\xi\eta$ system, the interface gap varies only with η and is related to g_s and $\theta_{b\xi}$ — the interface gap is not affected by the relative shear displacement or the relative twist rotation (which is a small-strain approximation). The interface gap is expressed in terms of s, t and β_s (by substituting the mapping of Eq. (19) into Eq. (20)):

$$g(\mathbf{r}) = g(s, t, \beta_s) = g_s + \left[t\cos\beta_s - s\sin\beta_s\right]\theta_{b\xi} = g_s + \left[t\xi_s - s\xi_t\right]\theta_{b\xi}$$

$$\text{with} \quad \theta_{b\xi} = \boldsymbol{\theta}_\mathbf{b} \cdot \hat{\boldsymbol{\xi}} = \|\boldsymbol{\theta}_\mathbf{b}\|, \quad \{s, t\} \in [-R, R] \tag{21}$$

$$\beta_s \in [0, 2\pi), \quad \xi_s = \hat{\boldsymbol{\xi}} \cdot \hat{\mathbf{s}}_\mathbf{c} = \cos\beta_s, \quad \xi_t = \hat{\boldsymbol{\xi}} \cdot \hat{\mathbf{t}}_\mathbf{c} = \sin\beta_s.$$

$$\theta_{b\xi} = \boldsymbol{\theta}_{\mathbf{b}} \cdot \hat{\boldsymbol{\xi}} = \left\| \boldsymbol{\theta}_{\mathbf{b}} \right\| > 0$$
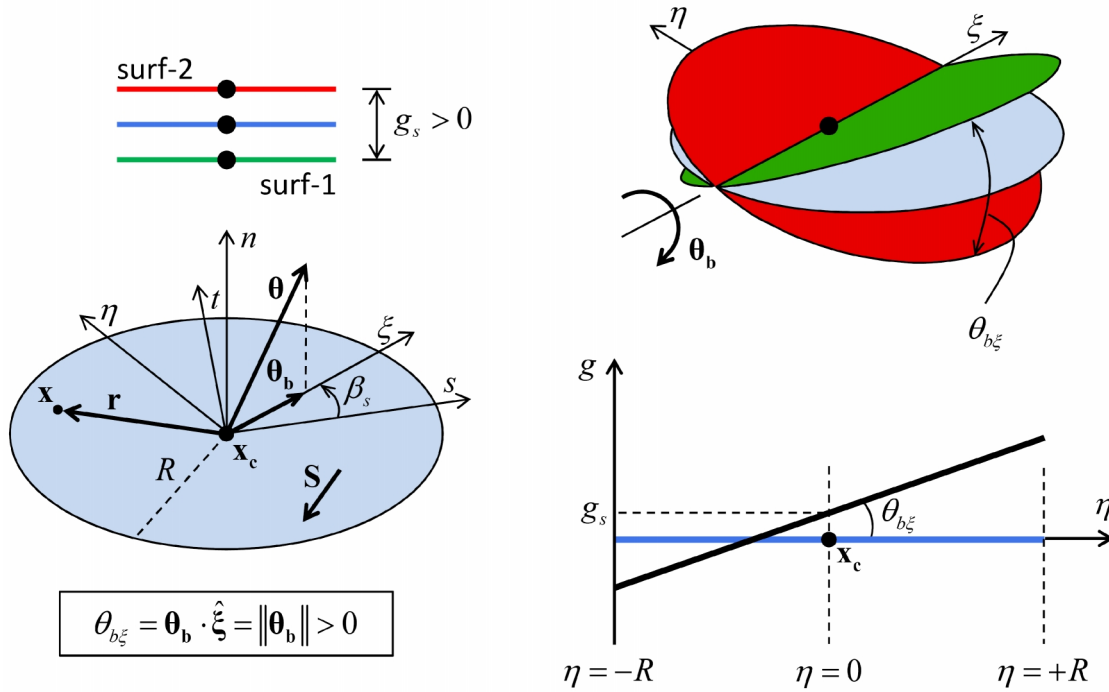
Figure 15 **Interface gap of the 3D flat-joint model corresponding with motion at top of image.**

For the 3D flat-joint model, the following components of the interface relative motion are tracked:

$$g_s := g_s + \Delta \delta_n$$
$$\delta_{ss} := \delta_{ss} + \Delta \boldsymbol{\delta}_{\mathbf{s}} \cdot \hat{\mathbf{s}}_{\mathbf{c}}, \ \ \delta_{st} := \delta_{st} + \Delta \boldsymbol{\delta}_{\mathbf{s}} \cdot \hat{\mathbf{t}}_{\mathbf{c}}$$
$$\theta_{bs} := \theta_{bs} + \Delta \boldsymbol{\theta}_{\mathbf{b}} \cdot \hat{\mathbf{s}}_{\mathbf{c}}, \ \ \theta_{bt} := \theta_{bt} + \Delta \boldsymbol{\theta}_{\mathbf{b}} \cdot \hat{\mathbf{t}}_{\mathbf{c}} \quad (22)$$
$$\xi_s = \begin{cases} 0, & \left\| \boldsymbol{\theta}_{\mathbf{b}} \right\| \le 1 \times 10^{-12} \\ \dfrac{\theta_{bs}}{\left\| \boldsymbol{\theta}_{\mathbf{b}} \right\|}, & \text{otherwise} \end{cases}, \ \xi_t = \begin{cases} 0, & \left\| \boldsymbol{\theta}_{\mathbf{b}} \right\| \le 1 \times 10^{-12} \\ \dfrac{\theta_{bt}}{\left\| \boldsymbol{\theta}_{\mathbf{b}} \right\|}, & \text{otherwise.} \end{cases}$$

1.6   Activity-Deletion Criterion

A contact with the flat-joint model is active if any element is either bonded or has a negative gap. The force-displacement law is skipped for inactive contacts. The contact may be deleted at the discretion of the cell-space logic if the distance between the centers of the notional surfaces becomes greater than the flat-joint diameter ($\sqrt{g_s^2 + (\delta_{ss})^2 + (\delta_{st})^2} > 2R$).

1.7 Force-Displacement Law

The force-displacement law for the flat-joint model updates the contact force and moment $\left(\mathbf{F_c} = \tilde{\mathbf{F}} \text{ and } \mathbf{M_c} = \tilde{\mathbf{M}} \right)$ that act at the contact location in an equal and opposite sense on the two pieces (see Figure 1). This is done by discretizing the interface into elements, and providing a force-displacement law for each element so that the force-displacement response of the flat-joint interface is an emergent behavior. The force-displacement law for a flat-joint element is described in this section.

Each element carries a force and moment $\left(\mathbf{F}^{(e)} \text{ and } \mathbf{M}^{(e)} \right)$ that act at the element centroid in an equal and opposite sense on the notional surfaces. The element forces and moments produce a statically equivalent force and moment at the center of the interface (which coincides with the contact location — see Figures 16 and 17) given by

$$\tilde{\mathbf{F}} = \sum_{\forall e} \mathbf{F}^{(e)}, \quad \tilde{\mathbf{M}} = \sum_{\forall e} \left\{ \left(\mathbf{r}^{(e)} \times \mathbf{F}^{(e)} \right) + \mathbf{M}^{(e)} \right\} \tag{23}$$

where $\mathbf{r}^{(e)} = \mathbf{x}^{(e)} - \mathbf{x_c}$ is the relative position and $\mathbf{x}^{(e)}$ is the centroid location of element (e). For the 2D model, Eq. (23) becomes:

$$\tilde{\mathbf{F}} = \sum_{\forall e} \mathbf{F}^{(e)}, \quad \tilde{\mathbf{M}} = \sum_{\forall e} \left\{ \left(\rho^{(e)} F_n^{(e)} \hat{\mathbf{k}} \right) + \mathbf{M}^{(e)} \right\} \quad \text{(2D model)} \tag{24}$$

by substituting $\mathbf{r}^{(e)}$ from Eq. (13) into Eq. (23) and expressing the element force in terms of its normal and shear components (defined below).
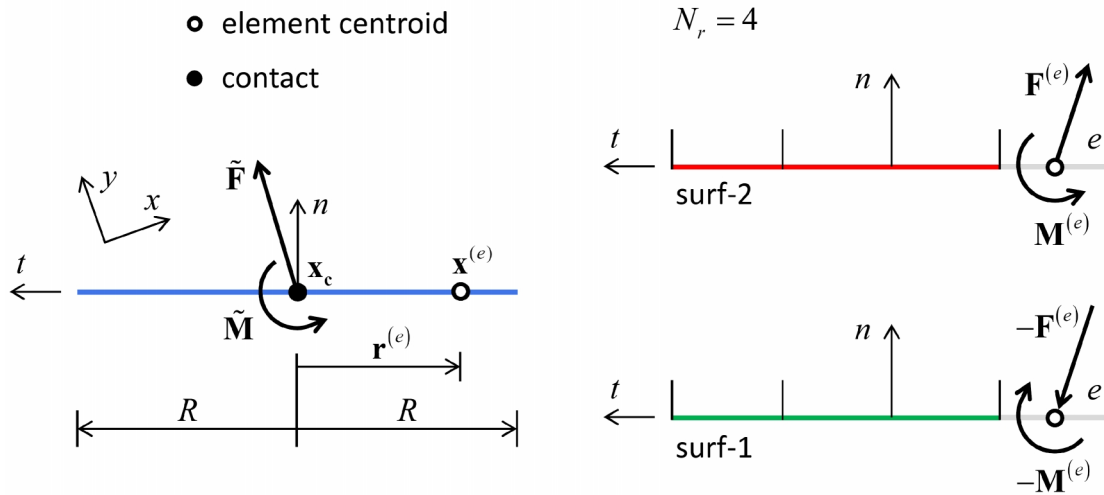
Figure 16 *Force and moment acting on a typical 2D element (right) and its centroid relative position vector used to determine their contribution to force and moment at the center of the interface (left).*

Figure 17 *Force and moment acting on a typical 3D element (right) and its centroid relative position vector used to determine their contribution to force and moment at the center of the interface (left).*
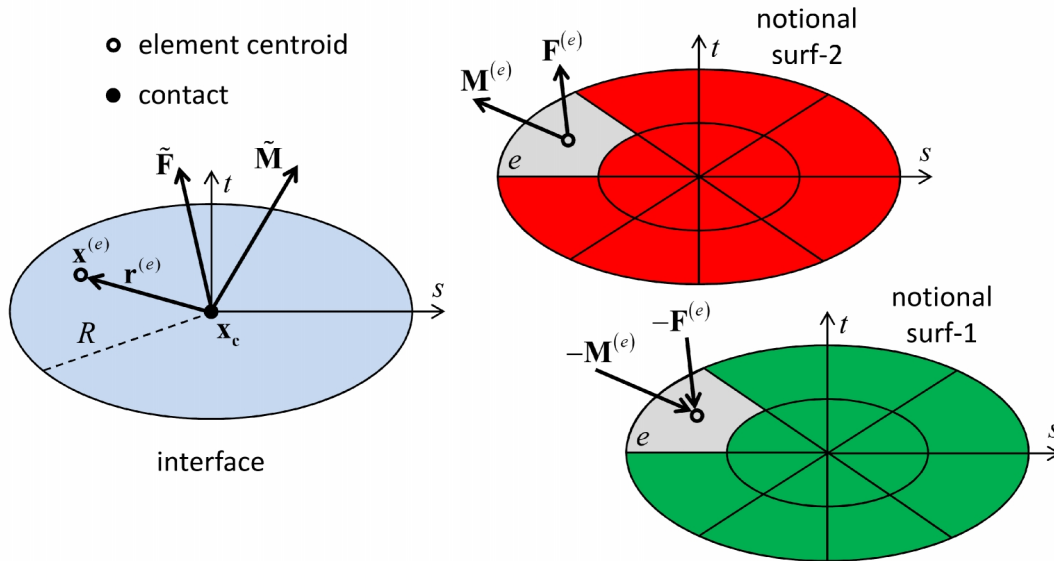
The force-displacement law for a flat-joint element updates the element force and moment $\left(\mathbf{F}^{(e)} \text{ and } \mathbf{M}^{(e)} \right)$ and may modify the element bond state ($B^{(e)}$). The element force is resolved into a normal and shear force, and the element moment is resolved into a twisting and bending moment:

$$\mathbf{F}^{(e)} = -F_n^{(e)} \hat{\mathbf{n}}_\mathbf{c} + \mathbf{F}_\mathbf{s}^{(e)}$$

$$\mathbf{M}^{(e)} = M_t^{(e)} \hat{\mathbf{n}}_\mathbf{c} + \mathbf{M}_\mathbf{b}^{(e)} \ \left(\text{2D model: } M_t^{(e)} \equiv 0\right) \tag{25}$$

where $F_n^{(e)} > 0$ is tension and $M_t^{(e)} > 0$ is shown in Figure 6. The shear force and bending moment lie on the interface and are expressed in the interface coordinate systems:

$$\mathbf{F}_\mathbf{s}^{(e)} = F_{ss}^{(e)} \hat{\mathbf{s}}_\mathbf{c} + F_{st}^{(e)} \hat{\mathbf{t}}_\mathbf{c} \ \left(\text{2D model: } F_{ss}^{(e)} \equiv 0\right)$$

$$\mathbf{M}_\mathbf{b}^{(e)} = M_b^{(e)} \begin{cases} \hat{\mathbf{k}}, & \text{2D} \\ \hat{\boldsymbol{\xi}}, & \text{3D.} \end{cases} \tag{26}$$

For the 3D model, a simplifying assumption[5] gives $M_t^{(e)} \equiv 0$. $F_n^{(e)}$ and $\mathbf{M}_\mathbf{b}^{(e)}$ are updated by integrating the normal stress acting over the element, and $\mathbf{F}_\mathbf{s}^{(e)}$ is updated incrementally based on the effective portion of the relative shear-displacement increment at the element centroid.

The element normal and shear stresses are given by

$$\sigma^{(e)} = \frac{F_n^{(e)}}{A^{(e)}}, \quad \tau^{(e)} = \frac{\left\| \mathbf{F}_\mathbf{s}^{(e)} \right\|}{A^{(e)}} \tag{27}$$

where $\sigma^{(e)} > 0$ is tension, and the stresses act at the element centroid. The interface normal stress $\left(\sigma, \ \sigma > 0 \text{ is tension}\right)$ is given by

$$\sigma(\mathbf{r}) = \begin{cases} 0, & \text{unbonded and } g(\mathbf{r}) \geq 0 \\ k_n g(\mathbf{r}), & \text{otherwise} \end{cases} \tag{28}$$

where k_n is the normal stiffness and g is the interface gap of Eqs. (14) and (21) for the 2D and 3D models, respectively. The interface normal stress is proportional to the gap, and the unbonded region with a positive gap carries no load — a tensile load is carried only in a bonded region with a positive gap, and a compressive load is carried wherever the gap is negative (regardless of its bonding state). The gap and normal stress are continuous over the interface, and the gap may change sign within an

---

[5] It is assumed that the shear stress arising from relative twist rotation is constant over the element and equal to its value at the element centroid. An inaccuracy introduced by this assumption is that the twisting moment is zero w.r.t. the element centroid. The interface shear stress arising from relative twist rotation actually varies linearly over the element, which makes the twisting moment non-zero w.r.t. the element centroid. As a result, the twisting moment at the center of the interface converges to the correct value from below as the discretization is refined. A similar assumption and associated inaccuracy exists for the bending moment of the 3D flat-joint model.

element; however, the bonding is not continuous over the interface because each element is either bonded or unbonded (see Figure 18).
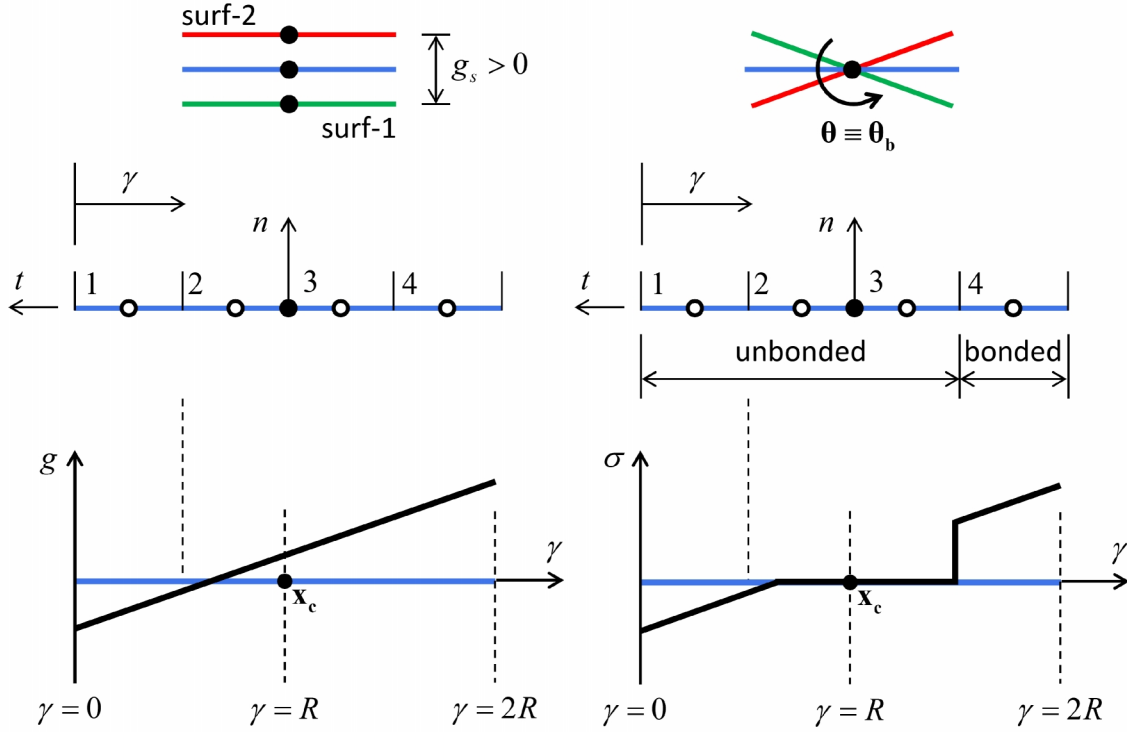

Figure 18   *Variation of gap, normal stress and bond state over a 4-element 2D flat-joint model corresponding with motion at top of image.*

When the flat-joint model is installed at a contact, initialize:

$$\forall e : \left\{ F_n^{(e)}, F_{ss}^{(e)}, F_{st}^{(e)}, M_b^{(e)} \right\} = \mathrm{E}_\mu^{(e)} = 0. \tag{29}$$

When the first cycle occurs after the flat-joint model is installed at a contact, fix the properties:

$$\left\{ N_r, N_\alpha, g_o \right\}, \quad R = \lambda \begin{cases} \min\left(R^{(1)}, R^{(2)} \right), \text{ ball-ball} \\ R^{(1)}, \text{ ball-wall} \end{cases} \tag{30}$$

and initialize:

$$\left\{ g_s = g_o, \quad \theta_{bs} = \theta_{bt} = 0 \right\} \text{ and } \left\{ \delta_{ss} = \delta_{st} = 0 \right\}. \tag{31}$$

The first condition establishes the initial location and orientation of the notional surfaces relative to the pieces. The initial surface gap (g_o, $g_o > 0$ is open) is the distance between the finite-size

notional surfaces measured along the dotted line in Figure 8. The surface gap ($g_s = g_o + \sum \Delta \delta_n$, $g_s > 0$ is open) is the cumulative relative normal displacement of the piece surfaces.

The force-displacement law for a flat-joint element consists of the following steps (see Figures 19 and 20).

1. Update $F_n^{(e)}$:

$$F_n^{(e)} = \int_e \sigma dA \tag{32}$$

   where σ is the interface normal stress of Eq. (28) and the integration is performed over element (e). Analytical expressions for this integral are used to update $F_n^{(e)}$, which in turn, is used to update $\sigma^{(e)} = F_n^{(e)} / A^{(e)}$. If the element is bonded and the tensile-strength limit is exceeded ($\sigma^{(e)} > \sigma_c$), then break the bond in tension $\left(B^{(e)} = 1, \{F_n^{(e)}, F_{ss}^{(e)}, F_{st}^{(e)}\} = 0 \right)$, trigger the **bond_break** call-back event and skip the next step. If the element is unbonded and $\sigma^{(e)} \geq 0$, then set the element shear force to zero $\left(\{F_{ss}^{(e)}, F_{st}^{(e)}\} = 0 \right)$ and skip the next step.

2. Update $\mathbf{F_s}^{(e)}$ as follows. Compute a trial element shear force:

$$\mathbf{F_s}^{(e)\prime} = \mathbf{F_s}^{(e)} - k_s A^{(e)} \Delta \widehat{\boldsymbol{\delta}}_s^{(e)\prime} \quad \left[F_{ss}^{(e)\prime} = F_{ss}^{(e)} - k_s A^{(e)} \Delta \widehat{\delta}_{ss}^{(e)\prime}, \ F_{st}^{(e)\prime} = F_{st}^{(e)} - k_s A^{(e)} \Delta \widehat{\delta}_{st}^{(e)\prime} \right]$$

$$\text{with } \Delta \widehat{\boldsymbol{\delta}}_s^{(e)\prime} = \alpha \Delta \widehat{\boldsymbol{\delta}}_s^{(e)} \quad \left[\Delta \widehat{\delta}_{ss}^{(e)\prime} = \alpha \Delta \widehat{\delta}_{ss}^{(e)}, \ \Delta \widehat{\delta}_{st}^{(e)\prime} = \alpha \Delta \widehat{\delta}_{st}^{(e)} \right] \tag{33}$$

$$\alpha = \begin{cases} \dfrac{g_1^{(e)}}{g_1^{(e)} - g_0^{(e)}}, & \text{unbonded and } g_0^{(e)} > 0 \text{ and } g_1^{(e)} < 0 \\ 1, & \text{otherwise} \end{cases}$$

   where $\Delta \widehat{\boldsymbol{\delta}}_s^{(e)\prime}$ is the effective portion of the relative shear-displacement increment at the element centroid. If the element is bonded, then the entire increment is effective; if the element is not bonded, then only the portion of the increment that occurs while $g^{(e)} < 0$ is effective; $\Delta \widehat{\boldsymbol{\delta}}_s^{(e)}$ is $\Delta \widehat{\boldsymbol{\delta}}_s$ of Eq. (12) evaluated at the element centroid and $g^{(e)}$ at the beginning and end of the time step is denoted by $g_0^{(e)}$ and $g_1^{(e)}$, respectively. The trial element shear stress:

$$\tau^{(e)\prime} = \left\| \mathbf{F}_\mathbf{s}^{(e)\prime} \right\| \Big/ A^{(e)} . \tag{34}$$

The procedure now differs based on the bond state as follows.

- **Unbonded**. The shear strength $\tau_c^{(e)} = -\mu \sigma^{(e)}$. If $\left| \tau^{(e)\prime} \right| \le \tau_c^{(e)}$, then $\mathbf{F}_\mathbf{s}^{(e)} = \mathbf{F}_\mathbf{s}^{(e)\prime}$; otherwise, enforce the shear-strength limit $\left(\mathbf{F}_\mathbf{s}^{(e)} = \tau_c^{(e)} A^{(e)} \left(\mathbf{F}_\mathbf{s}^{(e)\prime} \Big/ \left\| \mathbf{F}_\mathbf{s}^{(e)\prime} \right\| \right) \right)$, which implies that slip has occurred and the slip energy is updated via Eq. (39). If the slip state has changed, then trigger the **slip_change** call-back event.

- **Bonded**. The shear strength $\tau_c^{(e)} = c - \sigma^{(e)} \tan \phi$. If $\left| \tau^{(e)\prime} \right| \le \tau_c^{(e)}$, then $\mathbf{F}_\mathbf{s}^{(e)} = \mathbf{F}_\mathbf{s}^{(e)\prime}$; otherwise, the shear-strength limit has been exceeded: break the bond in shear (by setting $B^{(e)} = 2$, $\left\{ F_{ss}^{(e)}, F_{st}^{(e)} \right\} = 0$ and reevaluating $F_n^{(e)}$ as in step 1) and trigger the **bond_break** call-back event.

3. Update $M_b^{(e)}$:

$$M_b^{(e)} = -\int_e r\sigma dA \tag{35}$$

where σ is the interface normal stress of Eq. (28), r is the moment arm w.r.t. the element centroid and the integration is performed over element (e). Analytical expressions for this integral are used to update $M_b^{(e)}$.
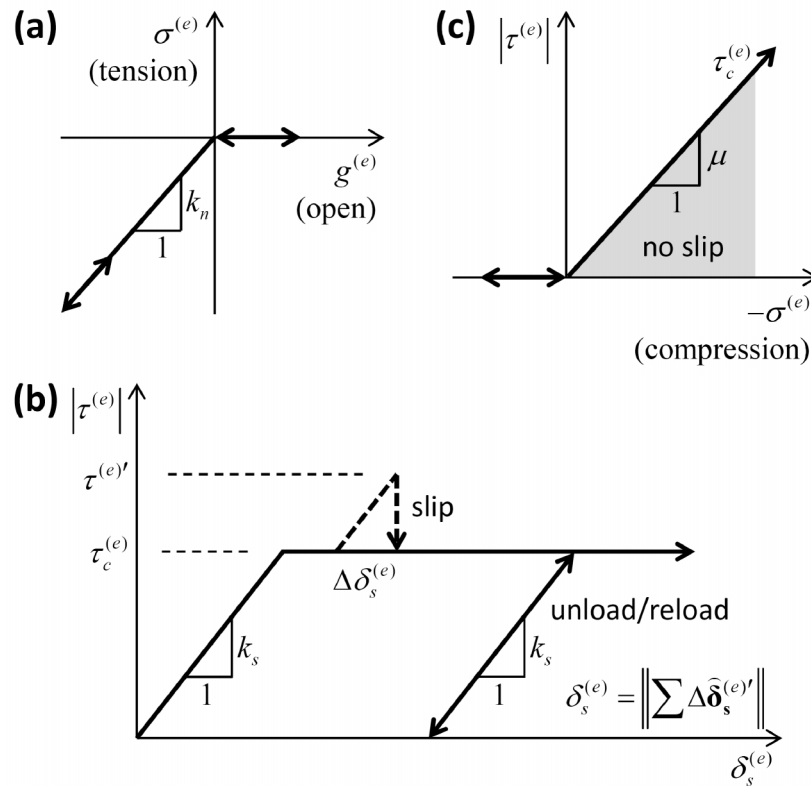
Figure 19 *Force-displacement law for an unbonded flat-joint element: (a) normal stress versus element gap, (b) shear stress versus relative shear displacement and (c) slip envelope.*

Figure 20   Force-displacement law for a bonded flat-joint element: (a) normal stress versus element gap, (b) shear stress versus relative shear displacement and (c) failure envelope.

1.8   Energy Partitions

The flat-joint model provides two energy partitions (see Table 2):

- strain energy, E_k, stored in the springs; and

- slip energy, E_μ, defined as the total energy dissipated by frictional slip.

Table 2   Flat-Joint Model Energy Partitions

Energy	Keyword	Description
E_k	**estrain**	strain energy
E_μ	**eslip**	total energy dissipated by slip

The strain energy in the flat joint is obtained by summing the strain energy in each element:

$$\mathrm{E}_k = \sum_{\forall e} \mathrm{E}_k^{(e)}. \tag{36}$$

The strain energy in each element is updated after the force-displacement law:

$$\mathrm{E}_k^{(e)} = \frac{1}{2} \left(\frac{\left(F_n^{(e)}\right)^2}{k_n A^{(e)}} + \frac{\left\|\mathbf{F}_s^{(e)}\right\|^2}{k_s A^{(e)}} + \frac{\left(M_b^{(e)}\right)^2}{k_n I^{(e)}} + \frac{\left(M_t^{(e)}\right)^2}{k_s J^{(e)}} \right)$$

$$\text{with} \quad I^{(e)} = \int_e \eta^2 dA = \begin{cases} \frac{2}{3} t \bar{r}^3, & \text{2D } (t=1) \\ \frac{1}{4} \pi r_e^4, & \text{3D} \end{cases} \tag{37}$$

$$J^{(e)} = \int_e \left(\xi^2 + \eta^2\right) dA = \begin{cases} 0, & \text{2D } (t=1) \\ \frac{1}{2} \pi r_e^4, & \text{3D} \end{cases}$$

$$r_e = \sqrt{A^{(e)}/\pi}$$

where $I^{(e)}$ is the moment of inertia of the element cross section (about the line passing through $\mathbf{x}^{(e)}$ and in the direction of $\mathbf{\theta_b}$) and $J^{(e)}$ is the polar moment of inertia of the element cross section (about the line through $\mathbf{x}^{(e)}$ and in the direction of $\hat{\mathbf{n}}_\mathbf{c}$), $\bar{r}$ is the element half-length and r_e is the element effective radius. The integrals in Eq. (37) are evaluated exactly for the 2D model, and approximated for the 3D model (by assuming that the element is a disk with an area equal to that of the element).

The slip energy in the flat joint is obtained by summing the slip energy in each element:

$$\mathrm{E}_\mu = \sum_{\forall e} \mathrm{E}_\mu^{(e)}. \tag{38}$$

The slip energy in each element is updated during the force-displacement law whenever the shear-strength limit has been exceeded via:

$$\mathrm{E}_\mu^{(e)} := \mathrm{E}_\mu^{(e)} + \tau_c^{(e)} A^{(e)} \left\| \Delta \hat{\mathbf{\delta}}_\mathbf{s}^{(e)\prime} \right\|. \tag{39}$$

1.9 Properties

The property information is separated into parameters and state variables such that the parameters define the model, while the state variables describe its current state. The properties table provides a concise property reference that combines the parameters and state variables. The property information for the flat-joint model is given in Tables 3–5.

Table 3 Flat-Joint Model Parameters

Parameter	Keyword	Description
	`flatjoint`	model name
N_r	`fj_Nr`	number of elements in radial direc. (2D model: number of elements)
N_α	`fj_Nal`	number of elements in circumferential direc. (3D model only, 2D model: $N_\alpha \equiv 1$)
λ	`fj_rmul`	radius multiplier
g_o	`fj_gap0`	initial surface gap
k_n	`fj_kn`	normal stiffness [stress/disp.]
k_s	`fj_ks`	shear stiffness [stress/disp.]
μ	`fj_fric`	friction coefficient
σ_c	`fj_ten`	tensile strength [stress]
c	`fj_coh`	cohesion [stress]
ϕ	`fj_fa`	friction angle [degrees]

Table 4 Flat-Joint Model State Variables

Variable	Keyword	Description
e	`fj_elem`	element (e) — accesses element-based data (element numbering in Figs. 12 and 14)
E^*	`fj_emod`	effective modulus
κ^*	`fj_kratio`	normal-to-shear stiffness ratio, $\kappa^* \equiv k_n / k_s$
$s^{(e)}$	`fj_slip`	slip state of element (e) $\left\{ \begin{array}{ll} \text{true,} & \text{slipping} \\ \text{false,} & \text{not slipping} \end{array} \right\}$
$B^{(e)}$	`fj_state`	bond state of element (e)

		$\begin{cases} 0, & \text{unbonded} \\ 1, & \text{unbonded \& broke in tension} \\ 2, & \text{unbonded \& broke in shear} \\ 3, & \text{bonded} \end{cases}$
R	`fj_radius`	flat-joint radius
g_s	`fj_gap`	surface gap
$\boldsymbol{\theta_b}$	`fj_relbr`	relative bend-rotation $\left(\theta_{bs}, \theta_{bt}\right)$ (2D model: $\theta_{bk} = -\theta_{bs}, \theta_{bt} \equiv 0$)
$\mathbf{x}^{(e)}$	`fj_cen`	centroid location of element (e)
$A^{(e)}$	`fj_area`	area of element (e)
$g^{(e)}$	`fj_egap`	gap at centroid of element (e)
$\tau_c^{(e)}$	`fj_shear`	shear strength [stress] at centroid of element (e)
$\sigma^{(e)}$	`fj_sigma`	normal stress at centroid of element (e)
$\tau^{(e)}$	`fj_tau`	shear stress at centroid of element (e)
$\tilde{\mathbf{F}}$	`fj_force`	interface force
$\tilde{\mathbf{M}}$	`fj_moment`	interface moment
T	`fj_mtype`	initial microstructural type $\begin{cases} 1, & \text{bonded} & (g_o = 0, \text{bonded}) \\ 2, & \text{gapped} & (g_o > 0, \text{unbonded}) \\ 3, & \text{slit} & (g_o = 0, \text{unbonded}) \\ 4, & \text{other} \end{cases}$

Table 5 Flat-Joint Model Properties

Name	Symbol	Range	Default	Type	Modifiable
`fj_Nr`	N_r	$[1, \infty)$	2	INT	no[1]
`fj_Nal`	N_α	$[3, \infty)$	4	INT	no[1]
`fj_rmul`	λ	$(0.0, \infty)$	1.0	FLT	no[1]
`fj_gap0`	g_o	$[0.0, \infty)$	0.0	FLT	no[1] $\left(\{g_o > 0\} \Rightarrow \left\{\forall e : B^{(e)} = 0\right\}\right)$
`fj_kn`	k_n	$[0.0, \infty)$	0.0	FLT	yes

`fj_ks`	k_s	$[0.0,\infty)$	0.0	FLT	yes
`fj_fric`	μ	$[0.0,\infty)$	0.0	FLT	yes
`fj_ten`	σ_c	$[0.0,\infty)$	0.0	FLT	yes
`fj_coh`	c	$[0.0,\infty)$	0.0	FLT	yes
`fj_fa`	ϕ	$[0.0,90.0)$	0.0	FLT	yes
`fj_elem`	e	$[1,N_r N_\alpha]$	1	INT	yes
`fj_emod`	E^*	$[0.0,\infty)$	0.0	FLT	no
`fj_kratio`	κ^*	$[0.0,\infty)$	0.0	FLT	no[2]
`fj_slip`	$s^{(e)}$	$\{\text{true},\text{false}\}$	false	BOOL[e]	no
`fj_state`	$B^{(e)}$	$\{0,1,2,3\}$	0	INT[e]	no
`fj_radius`	R	$(0,\infty)$	NA	FLT	no (set via λ)
`fj_gap`	g_s	$\mathbb{R}$	g_o	FLT	no
`fj_relbr`	$\boldsymbol{\theta}_b$	NA	**0**	VEC2	no
`fj_cen`	$\mathbf{x}^{(e)}$	NA	NA	VEC[e]	no
`fj_area`	$A^{(e)}$	$(0,\infty)$	NA	FLT[e]	no
`fj_egap`	$g^{(e)}$	$\mathbb{R}$	NA	FLT[e]	no
`fj_shear`	$\tau_c^{(e)}$	$[0.0,\infty)$	0.0	FLT	no (set via c and ϕ)
`fj_sigma`	$\sigma^{(e)}$	$\mathbb{R}$	NA	FLT[e]	no
`fj_tau`	$\tau^{(e)}$	$[0.0,\infty)$	NA	FLT[e]	no
`fj_force`	$\tilde{\mathbf{F}}$	$\mathbb{R}^3$	**0**	VEC	no
`fj_moment`	$\tilde{\mathbf{M}}$	$\mathbb{R}^3$	**0**	VEC	no
`fj_mtype`	T	$\{1,2,3,4\}$	NA	INT	no

[1] Specify before cycling, cannot modify thereafter.

[2] If either the normal or shear stiffness is zero, then κ^* is zero.

1.10 Methods

Methods allow one to perform an operation on a contact model, and some methods include parameters. The flat-joint model methods are listed in Table 6 and described as follows.

> **deformability.** The deformability provided by the flat-joint interface can be specified with the **deformability** method which sets:

$$k_n := E^*/L, \quad k_s := k_n/\kappa^*$$

$$\text{with} \quad L = \begin{cases} R^{(1)} + R^{(2)}, & \text{ball-ball} \\ R^{(1)}, & \text{ball-wall.} \end{cases} \tag{40}$$

The first term in this expression is obtained by equating the normal stiffness to the axial stiffness of the volume of material shown in Figure 21.
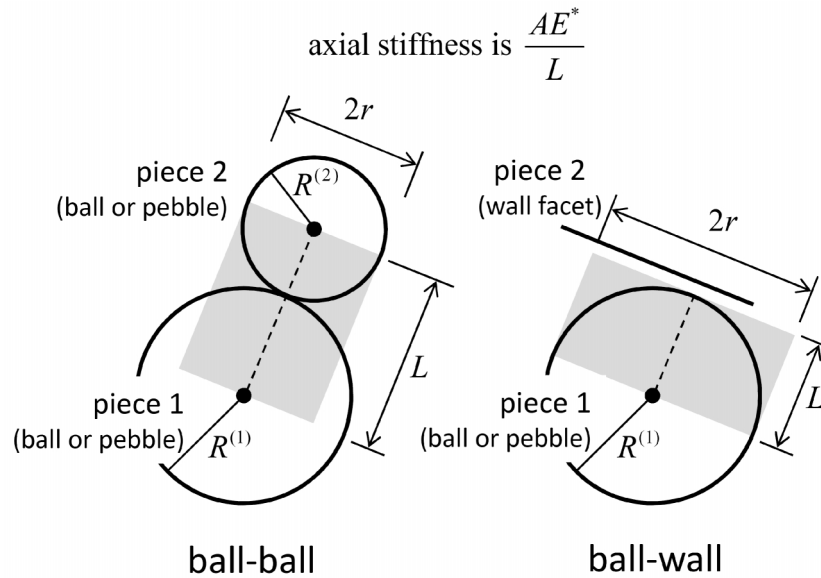

Figure 21 Volume of material associated with contact when setting deformability.

The deformability of a homogeneous, isotropic and well-connected granular assembly experiencing small-strain deformation can be fit by an isotropic material model, which is described by the elastic constants of Young's modulus (E) and Poisson's ratio (ν). E and ν are emergent properties that can be related to the effective modulus (E^*) and the normal-to-shear stiffness ratio ($\kappa^* \equiv k_n/k_s$) at the contact as follows: E is related to E^* with E increasing as E^* increases, and ν is related to κ^* with ν increasing up to a limiting positive value as κ^* increases. These relationships are obtained by specifying E^* and κ^* as the arguments of the **deformabilty** method.

bond. Bond element (e).[6] If the element number (e) is not specified, then bond all elements. Only elements with a zero gap over their entire surface can be bonded. If an element becomes bonded, then the element bond state becomes bonded ($B^{(e)} = 3$) — the element force and moment are unaffected and will be updated during the next cycle.

unbond. Unbond element (e). If the element number (e) is not specified, then unbond all elements. If the element becomes unbonded, then the element bond state becomes unbonded ($B^{(e)} = 0$) — the element force and moment are unaffected and will be updated during the next cycle.

Table 6   Flat-Joint Model Methods

Method	Argument	Description
deformability		Set deformability.
	emod	effective modulus (E^*)
	kratio	normal-to-shear stiffness ratio, $\kappa^* \equiv k_n / k_s$
bond		Bond element (e) or all elements.
	elem	element number (e) — element numbering in Figs. 12 and 14
unbond		Unbond element (e) or all elements.
	elem	element number (e) — element numbering in Figs. 12 and 14

1.11 Call-Back Events

Call-back events use the FISH call mechanism to associate the occurrence of an event (such as a bond breakage) with the calling of a FISH function. When the event occurs, the associated FISH function is called with information about the event passed into the function. The flat-joint model call-back events are listed in Table 7.

Table 7   Flat-Joint Model Call-Back Events

Event	Slot	Description
slip_change		Slip state of element (e) has changed.
	1	contact address
	2	element number (e) — element numbering in Figs. 12 and 14

---

[6] One can ensure the existence of contacts between all pieces with a contact gap less than a specified bonding gap (g_b) by specifying g_b as the proximity in the Contact Model Assignment Table.

		slip-change mode
	3	$\left\{ \begin{array}{l} 0, \ \text{slip has begun} \\ 1, \ \text{slip has ended} \end{array} \right\}$
bond_break		Bond of element (e) has broken.
	1	contact address
	2	element number (e) — element numbering in Figs. 12 and 14
		break mode
	3	$\left\{ \begin{array}{l} 0, \ \text{broke in tension} \\ 1, \ \text{broke in shear} \end{array} \right\}$

1.12 Stiffnesses for Time Step Estimation Scheme

The procedure to determine a stable time step (see Section 1.6 in the Theory & Background volume of Itasca [2008a&b]) requires that each contact model return the contact translational and rotational stiffnesses. For the flat-joint model, the translational stiffnesses are

$$\tilde{k}_n = k_n A, \quad \tilde{k}_s = k_s A$$
$$\text{with} \quad A = \left\{ \begin{array}{l} 2Rt, \ \ 2\text{D} \ (t = 1) \\ \pi R^2, \ \ 3\text{D} \end{array} \right. \tag{41}$$

and the rotational stiffnesses are

$$\tilde{k}_b = k_n I, \quad \tilde{k}_t = k_s J$$
$$\text{with} \quad I = \left\{ \begin{array}{l} \frac{2}{3} t R^3, \ \ 2\text{D} \ (t = 1) \\ \frac{1}{4} \pi R^4, \ \ 3\text{D} \end{array} \right. \quad \text{and} \quad J = \left\{ \begin{array}{l} 0, \ \ 2\text{D} \\ \frac{1}{2} \pi R^4, \ \ 3\text{D} \end{array} \right. \tag{42}$$

where A is the cross-sectional area, I is the moment of inertia and J is the polar moment of inertia of the entire flat-joint cross section.

1.13 Expressions for Element Normal Force and Bending Moment

Analytical expressions for the element normal force and bending moment ($F_n^{(e)}$ and $M_b^{(e)}$) are presented here. These expressions are obtained by integrating the interface normal stress over the element. The element normal force and bending moment satisfy:

$$F_n^{(e)} = \int_e \sigma dA$$

$$M_b^{(e)} = -\int_e r\sigma dA$$

(43)

where σ is the interface normal stress of Eq. (28), r is the moment arm w.r.t. the element centroid and the integration is performed over element (e). These integrals are evaluated exactly for the 2D model, and a simplifying assumption is made to evaluate them for the 3D model.

For the 2D model, the integrals are evaluated exactly as follows. The gap across the element (see Figure 22) is given by

$$g(\zeta) = g_a^{(e)} + \left(\frac{g_b^{(e)} - g_a^{(e)}}{2\bar{r}^{(e)}} \right)\zeta, \quad \zeta \in [0, 2\bar{r}]$$

(44)

where $g_a^{(e)}$ and $g_b^{(e)}$ are the values of the gap at the element ends (obtained by evaluating Eq. (14) at these locations) and $\bar{r}^{(e)}$ is the element half-length.
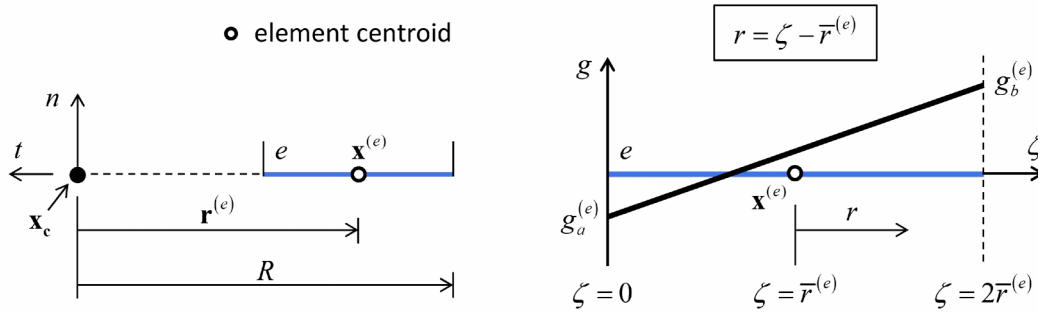

Figure 22   Variation of interface gap over a typical 2D element.

The element is mapped into one of the following three cases (considered in order): (1) the gap changes sign within the element ($g_a^{(e)} g_b^{(e)} < 0$); (2) the gap remains positive or zero $\left(g_a^{(e)} \geq 0 \text{ and } g_b^{(e)} \geq 0 \right)$; or (3) the gap remains negative ($g_a^{(e)} \leq 0$ and $g_b^{(e)} \leq 0$).

The integrals in Eq. (43) are expressed in the element system by

$$F_n^{(e)} = \int_0^{2\bar{r}} \sigma t d\zeta \quad (t = 1)$$

$$M_b^{(e)} = -\int_0^{2\bar{r}} r\sigma t d\zeta \quad (t = 1), \quad r = \zeta - \bar{r}^{(e)}.$$

(45)

where the $g(\mathbf{r})$ term of the interface normal stress of Eq. (28) is expressed via Eq. (44). These integrals are evaluated analytically for each case to yield (with the superscript-(e) notation dropped for the g_a, g_b and $\bar{r}$ terms):

$$\text{case 1: } F_n^{(e)} = k_n \bar{r} t \begin{cases} g_a + g_b, & \text{bonded} \\ \dfrac{g_a^2}{g_a - g_b}, & \text{unbonded and } g_a < 0 \\ \dfrac{g_b^2}{g_b - g_a}, & \text{unbonded and } g_a > 0 \end{cases} \tag{46}$$

$$\text{case 1: } M_b^{(e)} = k_n \bar{r}^2 t \begin{cases} \dfrac{g_a - g_b}{3}, & \text{bonded} \\ \dfrac{g_a^2 (g_a - 3g_b)}{3(g_b - g_a)^2}, & \text{unbonded and } g_a < 0 \\ \dfrac{-(g_b - g_a)^3 - g_a^2 (g_a - 3g_b)}{3(g_b - g_a)^2}, & \text{unbonded and } g_a > 0 \end{cases} \tag{47}$$

$$\text{case 2: } \begin{aligned} F_n^{(e)} &= k_n \bar{r} t \begin{cases} g_a + g_b, & \text{bonded} \\ 0, & \text{unbonded} \end{cases} \\ M_b^{(e)} &= k_n \bar{r}^2 t \begin{cases} \dfrac{g_a - g_b}{3}, & \text{bonded} \\ 0, & \text{unbonded} \end{cases} \end{aligned} \tag{48}$$

$$\text{case 3: } \begin{aligned} F_n^{(e)} &= k_n \bar{r} t (g_a + g_b) \\ M_b^{(e)} &= k_n \bar{r}^2 t \left(\dfrac{g_a - g_b}{3} \right). \end{aligned} \tag{49}$$

For the 3D model, it is assumed that the normal stress is constant over the element and equal to its value at the element centroid[7] such that

---

[7] An inaccuracy introduced by this assumption is that the bending moment is zero w.r.t. the element centroid. The interface normal stress actually varies linearly over the element, which makes the bending moment non-zero w.r.t. the element centroid. As a result, the bending moment at the center of the interface converges to the correct value from

$$F_n^{(e)} = \int_e \sigma dA = \begin{cases} 0, & \text{unbonded and } g^{(e)} \geq 0 \\ k_n g^{(e)} A^{(e)}, & \text{otherwise} \end{cases}$$

$$M_b^{(e)} = -\int_e r\sigma dA = 0$$

(50)

where $g^{(e)}$ is the gap at the element centroid obtained by evaluating Eq. (21) at the element centroid.

below as the discretization is refined. A similar assumption and associated inaccuracy exists for the twisting moment of the 3D flat-joint model.

2.0   TEST PROBLEMS

Flat-joint contact model test problems of two grains and an interlocked grain are provided in the following subsections. An example of a flat-jointed material is provided in Potyondy (2016, Example Materials 2: Flat-Jointed Material Example). There is a test project for each test problem, and these projects are in the **fistPkgN/ExampleProjects/FlatJointContactModel** directory, where **N** is the version number of the material-modeling support package. There are separate 2D and 3D projects for each test problem, and both projects are contained within the same example-project directory.

2.1   Behavior of a Flat Joint

The behavior of a single flat-joint contact is studied via the two-grain test problem in the **Test-TwoGrains** example-project directory. The problem is shown in Figure 23 and described as follows. Two granite grains (modeled in 3D as gravel-sized spheres) are stacked one atop the other such that they are just touching. The motion of both grains is fully specified, with a different motion for each of the three loading cases, which correspond with pure axial, twisting and bending loads. The two-grain test problem is modeled with both the linear parallel bond and the flat joint contact models. The elastic responses will be similar for a fully bonded flat-joint contact and a parallel-bonded contact with an intact bond, and closed-form expressions for these responses are presented. The contact-model properties are chosen to correspond with those of an elastic beam of granite that joins the grain centers, with beam radius equal to the flat-joint and parallel-bond radii.[8] The density (ρ), Young's modulus (E) and Poisson's ratio (ν) of granite are $2650 \ \mathrm{kg/m^3}$, $29\,\mathrm{GPa}$ and 0.15, respectively. Quasi-static conditions are enforced via local-damping, with a local-damping factor (α) of 0.7.

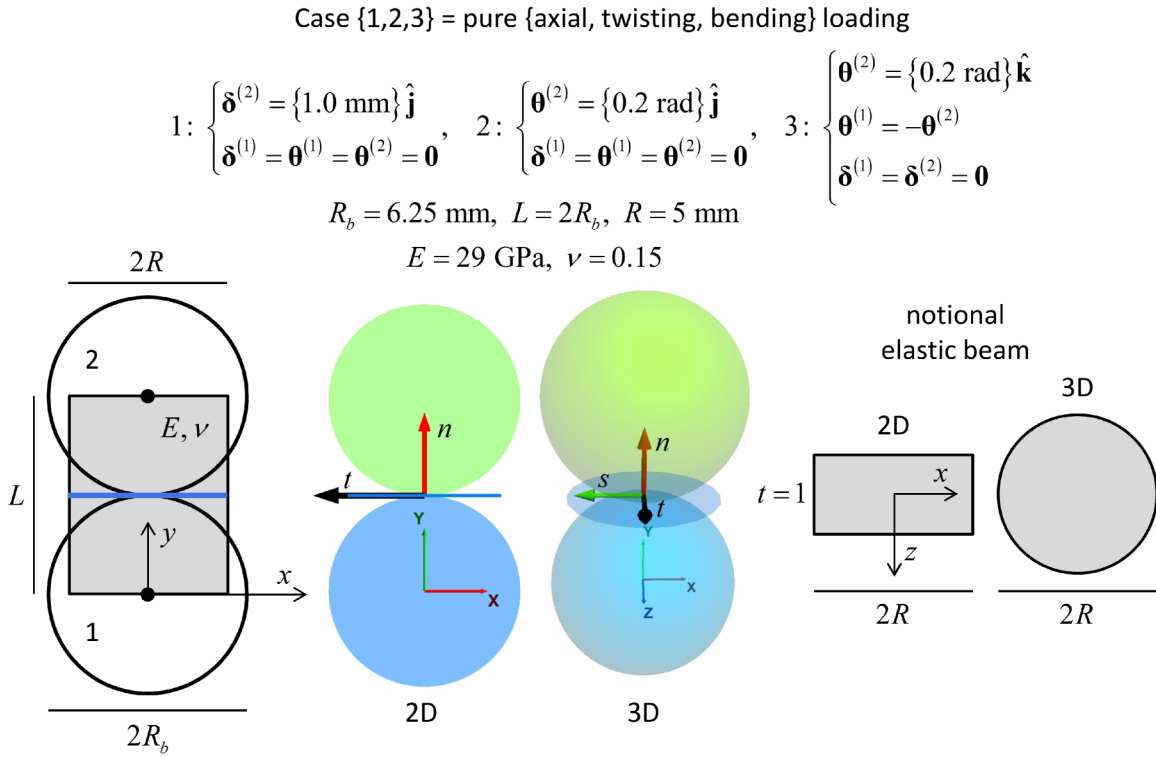[8] The beam has a rectangular and circular cross section, for the 2D and 3D models, respectively.

Case {1,2,3} = pure {axial, twisting, bending} loading

$$1: \begin{cases} \boldsymbol{\delta}^{(2)} = \{1.0 \text{ mm}\}\, \hat{\mathbf{j}} \\ \boldsymbol{\delta}^{(1)} = \boldsymbol{\theta}^{(1)} = \boldsymbol{\theta}^{(2)} = \mathbf{0} \end{cases}, \quad 2: \begin{cases} \boldsymbol{\theta}^{(2)} = \{0.2 \text{ rad}\}\, \hat{\mathbf{j}} \\ \boldsymbol{\delta}^{(1)} = \boldsymbol{\theta}^{(1)} = \boldsymbol{\theta}^{(2)} = \mathbf{0} \end{cases}, \quad 3: \begin{cases} \boldsymbol{\theta}^{(2)} = \{0.2 \text{ rad}\}\, \hat{\mathbf{k}} \\ \boldsymbol{\theta}^{(1)} = -\boldsymbol{\theta}^{(2)} \\ \boldsymbol{\delta}^{(1)} = \boldsymbol{\delta}^{(2)} = \mathbf{0} \end{cases}$$

$$R_b = 6.25 \text{ mm}, \quad L = 2R_b, \quad R = 5 \text{ mm}$$
$$E = 29 \text{ GPa}, \quad \nu = 0.15$$

Figure 23   Two-grain test problem.

2.1.1   Closed-form solutions

The closed-form solutions provide values for $\mathbf{F}^{(g)}$ and $\mathbf{M}^{(g)}$, the externally applied force and moment, respectively, acting on grain (g). These externally applied loads arise in response to the imposed motion, and are resisted by the contact force and moment ($\mathbf{F}_c$ and $\mathbf{M}_c$ shown in Figure 1) that act in an equal and opposite sense on the two grains. The contact force and moment are considered to be an internal load in the two-grain system. The internal and external loads in the two-grain system are related to one another via

$$\mathbf{F}^{(1)} = -\mathbf{F}^{(2)} = \mathbf{F}_c, \quad \mathbf{M}^{(1)} = -\mathbf{M}^{(2)} = \mathbf{M}_c. \tag{51}$$

Closed-form expressions for the axial, twisting and bending stiffnesses of an elastic beam of length L loaded at its ends by equal and opposite normal forces, twisting and bending moments, respectively, are given by

$$F_n = k_n \Delta_n, \quad k_n = \frac{AE}{L}$$

$$M_t = k_t \theta_t, \quad k_t = \frac{GJ}{L} \tag{52}$$

$$M_b = k_b \theta_b, \quad k_b = \frac{EI}{L}$$

where E and G are the Young's modulus and shear modulus, respectively, of the beam; A is the cross-sectional area of the beam; J is the polar moment of inertia of the beam cross section; and I is the moment of inertia of the beam cross section.

The closed-form solution for Case 1 (pure axial load):

$$F_n = k_n \Delta_n = \left(\frac{AE}{L}\right)\Delta_n \cong \begin{cases} 2.3200 \times 10^7 \text{ N, 2D} \\ 1.8221 \times 10^5 \text{ N, 3D} \end{cases}$$

$$\text{with } A = \begin{cases} 2Rt, \text{ 2D } (t=1) \\ \pi R^2, \text{ 3D} \end{cases}, \quad \Delta_n = 1 \text{ mm} \tag{53}$$

$$\mathbf{F}^{(1)} = -\mathbf{F}^{(2)} = -F_n \hat{\mathbf{j}}, \quad \mathbf{M}^{(1)} = \mathbf{M}^{(2)} = \mathbf{0}.$$

The closed-form solution for Case 2 (pure twisting load):

$$M_t = k_t \theta_t = \left(\frac{GJ}{L}\right)\theta_t = \left(\frac{EJ}{2(1+v)L}\right)\theta_t = \theta_t \cong \begin{cases} \text{NA, 2D} \\ 1.9806 \times 10^2 \text{ Nm, 3D} \end{cases}$$

$$\text{with } J = \begin{cases} \text{NA, 2D} \\ \frac{1}{2}\pi R^4, \text{ 3D} \end{cases}, \quad \theta_t = 0.2 \text{ rad} \tag{54}$$

$$\mathbf{F}^{(1)} = \mathbf{F}^{(2)} = \mathbf{0}, \quad \mathbf{M}^{(1)} = -\mathbf{M}^{(2)} = -M_t \hat{\mathbf{j}}.$$

The closed-form solution for Case 3 (pure bending load):

$$M_b = k_b \theta_b = \left(\frac{EI}{L}\right)\theta_b \cong \begin{cases} 7.7333 \times 10^4 \text{ Nm, } 2\text{D} \\ 4.5553 \times 10^2 \text{ Nm, } 3\text{D} \end{cases}$$

$$\text{with } I = \begin{cases} \frac{2}{3}tR^3, \ 2\text{D} \ (t=1) \\ \frac{1}{4}\pi R^4, \ 3\text{D} \end{cases}, \ \theta_b = \left|\theta_b^{(2)} - \theta_b^{(1)}\right| = 0.4 \text{ rad} \tag{55}$$

$$\mathbf{F}^{(1)} = \mathbf{F}^{(2)} = \mathbf{0}, \ \mathbf{M}^{(1)} = -\mathbf{M}^{(2)} = -M_b\hat{\mathbf{k}}.$$

2.1.2   Model properties (parallel-bonded contact)

The parallel-bonded contact has properties:

$$k_n = k_s = 0 \quad \left(\text{linear force is zero, } \mathbf{F^l} = \mathbf{0}\right)$$

$$\beta_n = \beta_s = 0 \quad \left(\text{dashpot force is zero, } \mathbf{F^d} = \mathbf{0}\right)$$

$$\overline{\lambda} = 0.8 \Rightarrow \overline{R} = 5 \text{ mm}, \ \overline{\beta} = 1$$

$$\overline{B} = 3, \ \overline{\sigma}_c = \overline{c} = 1 \times 10^{20} \text{ N/m}^2, \ \overline{\phi} = 0 \ \left(\text{intact bond, infinite strength}\right) \tag{56}$$

$$\overline{k}_n = \frac{E}{L} = \frac{29 \times 10^9 \text{ N/m}^2}{12.5 \times 10^{-3} \text{ m}} = 2.3200 \times 10^{12} \text{ N/m}^3$$

$$\overline{k}_s = \frac{G}{L} = \frac{E}{2(1+v)L} = \frac{29 \times 10^9 \text{ N/m}^2}{2(1+0.15)12.5 \times 10^{-3} \text{ m}} \cong 1.0087 \times 10^{12} \text{ N/m}^3$$

where the relation for $\overline{k}_n$ insures that we match both the axial and bending stiffnesses, and the relation for $\overline{k}_s$ insures that we match the twisting stiffness of the elastic beam.

The parallel-bonded contact has cross-sectional properties:

$$\overline{R} = \overline{\lambda} \min\left(R^{(1)}, R^{(2)}\right) = R = 5.0 \times 10^{-3} \text{ m}$$

$$\overline{A} = A, \ \overline{I} = I, \ \overline{J} = J \tag{57}$$

where expressions for A, I and J are given above in the closed-form solution section.

2.1.3   Model response (parallel-bonded contact)

The expected contact force and moment for the parallel-bonded contact follows. The expected contact values correspond exactly with the closed-form solutions. The modeled-system response matches these values exactly.

For the parallel-bonded contact:

$$\mathbf{F_c} = \overline{\mathbf{F}} = -F_n\,\hat{\mathbf{n}}_\mathbf{c} + \mathbf{F_s} = -\overline{F}_n\,\hat{\mathbf{n}}_\mathbf{c} + \overline{F}_{ss}\,\hat{\mathbf{s}}_\mathbf{c} + \overline{F}_{st}\,\hat{\mathbf{t}}_\mathbf{c}\quad\left(\text{2D model: } \overline{F}_{ss} \equiv 0\right)$$

$$\mathbf{M_c} = \overline{\mathbf{M}} = \overline{M}_t\,\hat{\mathbf{n}}_\mathbf{c} + \overline{\mathbf{M}}_\mathbf{b} = \overline{M}_t\,\hat{\mathbf{n}}_\mathbf{c} + \overline{M}_{bs}\,\hat{\mathbf{s}}_\mathbf{c} + \overline{M}_{bt}\,\hat{\mathbf{t}}_\mathbf{c}\quad\left(\text{2D model: } \overline{M}_t \equiv \overline{M}_{bt} \equiv 0\right)$$

(58)

where $\overline{\mathbf{F}}$ and $\overline{\mathbf{M}}$ are the parallel-bond force and moment, respectively.

Expected contact force and moment (parallel-bonded contact, Case 1):

$$\overline{F}_n = \overline{k}_n\,\overline{A}\,\overline{g}_s \cong \begin{cases} 2.3200\times10^7 \text{ N, 2D} \\ 1.8221\times10^5 \text{ N, 3D} \end{cases}, \quad \overline{g}_s = 1 \text{ mm}$$

$$\overline{F}_{ss} = \overline{F}_{st} = \overline{M}_t = \overline{M}_{bs} = \overline{M}_{bt} = 0.$$

(59)

Expected contact force and moment (parallel-bonded contact, Case 2):

$$\overline{M}_t = -\overline{k}_s\,\overline{J}\left(\theta_t^{(2)} - \theta_t^{(1)}\right) \cong \begin{cases} \text{NA, 2D} \\ -1.9806\times10^2 \text{ Nm, 3D} \end{cases}, \quad \theta_t^{(2)} - \theta_t^{(1)} = 0.2 \text{ rad}$$

$$\overline{F}_n = \overline{F}_{ss} = \overline{F}_{st} = \overline{M}_{bs} = \overline{M}_{bt} = 0.$$

(60)

Expected contact force and moment (parallel-bonded contact, Case 3):

$$\begin{cases} \overline{M}_{bs} = -\overline{k}_n\,\overline{I}\left(\theta_{bs}^{(2)} - \theta_{bs}^{(1)}\right) = -7.7333\times10^4 \text{ Nm, } \theta_{bs}^{(2)} - \theta_{bs}^{(1)} = -0.4 \text{ rad} \\ \overline{F}_n = \overline{F}_{ss} = \overline{F}_{st} = \overline{M}_t = \overline{M}_{bt} = 0 \end{cases}, \text{2D} \\ \begin{cases} \overline{M}_{bt} = -\overline{k}_n\,\overline{I}\left(\theta_{bt}^{(2)} - \theta_{bt}^{(1)}\right) = -4.5553\times10^2 \text{ Nm, } \theta_{bt}^{(2)} - \theta_{bt}^{(1)} = 0.4 \text{ rad} \\ \overline{F}_n = \overline{F}_{ss} = \overline{F}_{st} = \overline{M}_t = \overline{M}_{bs} = 0 \end{cases}, \text{ 3D.}$$

(61)

2.1.4 Model properties (flat-jointed contact)

The flat-jointed contact has properties:

$$\{N_r, N_\alpha\} = \begin{cases} \{4,1\}, \text{ 2D} \\ \{2,8\}, \text{ 3D} \end{cases}, \quad \lambda = 0.8 \Rightarrow R = 5 \text{ mm}, \quad g_o = 0, \quad \mu = 0$$

$$B^{(e)} = 3\,(\forall e), \quad \sigma_c = c = 1\times10^{20} \text{ N/m}^2, \quad \phi = 0 \quad \text{(fully bonded, infinite strength)}$$

$$k_n = \frac{E}{L} = \frac{29\times10^9 \text{ N/m}^2}{12.5\times10^{-3} \text{ m}} = 2.3200\times10^{12} \text{ N/m}^3$$

$$k_s = \frac{G}{L} = \frac{E}{2(1+\nu)L} = \frac{29\times10^9 \text{ N/m}^2}{2(1+0.15)12.5\times10^{-3} \text{ m}} \cong 1.0087\times10^{12} \text{ N/m}^3$$

(62)

where the relation for k_n insures that we match both the axial and bending stiffnesses, and the relation for k_s insures that we match the twisting stiffness of the elastic beam.

2.1.5   Model response (flat-jointed contact)

The modeled-system response of the flat-jointed contact matches the closed-form solutions for force and moment applied to the grains for Case 1. The response of the 2D flat-jointed contact also matches the closed-form solution for Case 3; however, the response of the 3D flat-jointed contact converges to the Case 2 and 3 values from below as the discretization is refined. Note that Case 2 is only relevant to the 3D model. The error in the contact twisting moment (revealed by Case 2) arises from the assumption that the shear stress induced by relative twist rotation is constant over each element, when in fact the shear stress varies linearly over each element (see footnote 5). The error in the contact bending moment of the 3D model arises from the assumption that the normal stress induced by bending is constant over each element and equal to its value at the element centroid, when in fact, the normal stress varies linearly over each element (see footnote 7). This assumption was not made for the 2D model, which instead evaluated exactly the integrals of normal stress that give element normal force and bending moment. It is expected that these integrals could also be evaluated exactly for the 3D model, which would remove the errors in the contact twisting and bending moments.

For the flat-jointed contact:

$$\mathbf{F_c} = \tilde{\mathbf{F}} = \sum_{\forall e} \mathbf{F}^{(e)}, \quad \mathbf{M_c} = \tilde{\mathbf{M}} = \sum_{\forall e} \left\{ \left(\mathbf{r}^{(e)} \times \mathbf{F}^{(e)} \right) + \mathbf{M}^{(e)} \right\} \tag{63}$$

where $\tilde{\mathbf{F}}$ and $\tilde{\mathbf{M}}$ are the interface force and moment, respectively.

Measured contact force and moment (flat-jointed contact, Case 1):

$$\tilde{F}_n = \begin{cases} 2.3200 \times 10^7 \text{ N,} & \text{2D} \\ 1.8221 \times 10^5 \text{ N,} & \text{3D} \end{cases} \tag{64}$$

$$\tilde{F}_{ss} = \tilde{F}_{st} = \tilde{M}_t = \tilde{M}_{bs} = \tilde{M}_{bt} = 0.$$

Measured contact force and moment (flat-jointed contact, Case 2):

$$\tilde{M}_t = \begin{cases} \text{NA, 2D} \\ -1.8112 \times 10^2 \text{ Nm, 3D} \left(\{N_r, N_\alpha\} = \{2,8\} \right) \\ -1.9211 \times 10^2 \text{ Nm, 3D} \left(\{N_r, N_\alpha\} = \{3,16\} \right) \\ -1.9495 \times 10^2 \text{ Nm, 3D} \left(\{N_r, N_\alpha\} = \{4,24\} \right) \\ -1.9806 \times 10^2 \text{ Nm, 3D (closed-form solution)} \end{cases} \tag{65}$$

$$\tilde{F}_n = \tilde{F}_{ss} = \tilde{F}_{st} = \tilde{M}_{bs} = \tilde{M}_{bt} \cong 0.$$

Measured contact force and moment (flat-jointed contact, Case 3):

$$\begin{cases} \begin{aligned} \tilde{M}_{bs} &= -7.7333 \times 10^4 \text{ Nm} \\ \tilde{F}_n = \tilde{F}_{ss} = \tilde{F}_{st} = \tilde{M}_t &= \tilde{M}_{bt} = 0 \end{aligned} &, \text{ 2D} \\ \\ \tilde{M}_{bt} = \begin{cases} -4.1657 \times 10^2 \text{ Nm}, & \{N_r, N_\alpha\} = \{2,8\} \\ -4.4185 \times 10^2 \text{ Nm}, & \{N_r, N_\alpha\} = \{3,16\} \\ -4.4838 \times 10^2 \text{ Nm}, & \{N_r, N_\alpha\} = \{4,24\} \\ -4.5553 \times 10^2 \text{ Nm}, & \text{closed-form solution} \end{cases} &, \text{ 3D.} \\ \\ \quad\quad \tilde{F}_n = \tilde{F}_{ss} = \tilde{F}_{st} = \tilde{M}_t = \tilde{M}_{bs} \cong 0 \end{cases} \tag{66}$$

2.2 Behavior of an Interlocked Grain

The behavior of an interlocked grain is studied via the interlocked-grain test problem in the **Test-InterlockedGrain** example-project directory. The two- and three-dimensional problems are shown in Figures 24 and 25, respectively. The particles are aligned with each other such that they are just touching. The flat-joint contact model is installed at the four contacts and assigned the following properties (slightly modified from those in the preceding section):

$$\{N_r, N_\alpha\} = \begin{cases} \{4,1\}, & \text{2D} \\ \{2,8\}, & \text{3D} \end{cases}, \ \lambda = 0.8 \Rightarrow R = 5 \text{ mm}, \ g_o = 0, \ \mu = 0$$

$$B^{(e)} = 0 \ (\forall e), \ \sigma_c = c = \phi = 0 \ \left(\text{fully unbonded}\right) \tag{67}$$

$$k_n = 2.3200 \times 10^{12} \text{ N/m}^3$$

$$k_s = 1.0087 \times 10^{12} \text{ N/m}^3$$

such that the interfaces are unbonded and frictionless. First, the central grain is rotated counter-clockwise while keeping the surrounding grains fixed in all DOFs (translational and rotational velocities are fixed to zero). A compressive force develops at the far end of each of the four faces,

and these forces resist the moment applied to the central grain. Next, the motion of the central grain is stopped, and the rotational restraint on the surrounding grains is removed. The surrounding grains rotate to accommodate the imposed rotation of the inner grain.
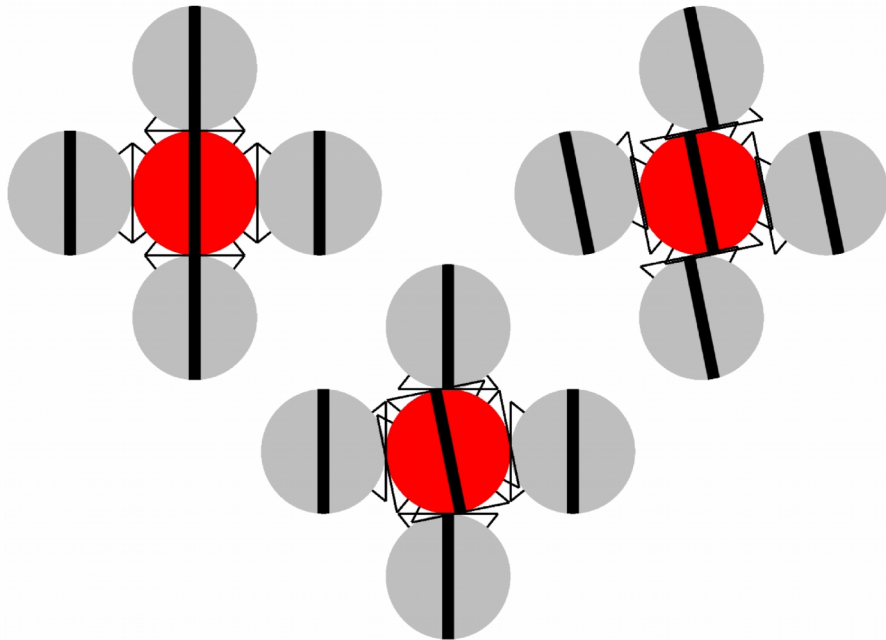

Figure 24   Interlocked-grain test problem in 2D. Faced grains before (left) and after (center) the imposed motion and after releasing rotational restraint on the surrounding grains (right).
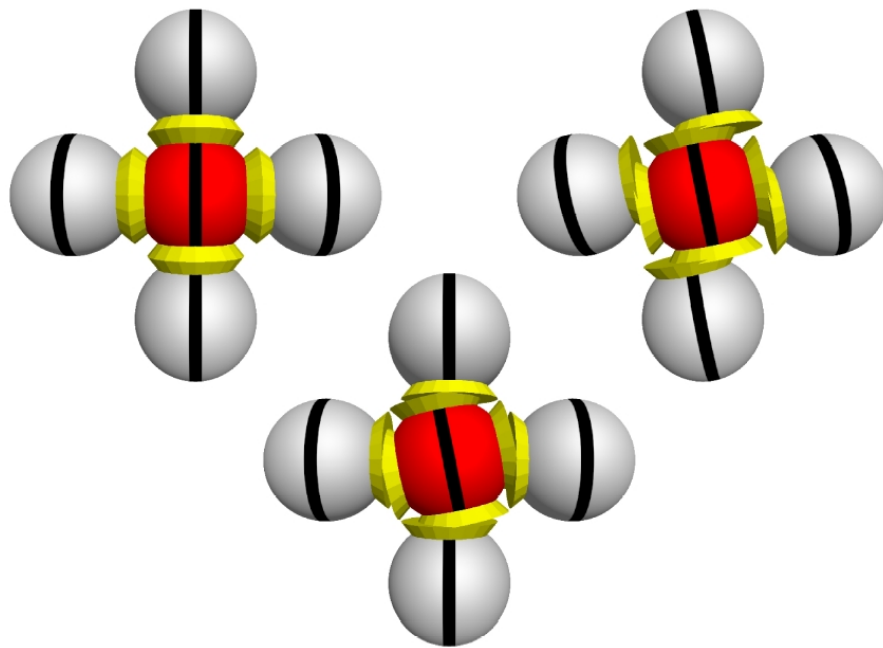
Figure 25 ***Interlocked-grain test problem in 3D. Faced grains before (left) and after (center) the imposed motion and after releasing rotational restraint on the surrounding grains (right).***

3.0   REFERENCES

Itasca Consulting Group, Inc. (2008a) *PFC3D — Particle Flow Code in 3 Dimensions*, Version 4.0, User's Manual. Minneapolis: Itasca.

Itasca Consulting Group, Inc. (2008b) *PFC2D — Particle Flow Code in 2 Dimensions*, Version 4.0, User's Manual. Minneapolis: Itasca.

Itasca Consulting Group, Inc. (2016) *PFC — Particle Flow Code in 2 and 3 Dimensions*, Version 5.0, Documentation Set of version 5.00.27 [September 5, 2016]. Minneapolis: Itasca.

Potyondy, D. (2016) "Material-Modeling Support in PFC [fistPkg24]," Itasca Consulting Group, Inc., Technical Memorandum ICG7766-L (October 12, 2016), Minneapolis, Minnesota.

Potyondy, D. O. (2015) "The Bonded-Particle Model as a Tool for Rock Mechanics Research and Application: Current Trends and Future Directions," *Geosystem Engineering, 18(1)*, 1–28.

Potyondy, D. (2013) "*PFC3D* Flat-Joint Contact Model (version 1)," Itasca Consulting Group, Inc., Minneapolis, MN, Technical Memorandum ICG7234-L, June 25, 2013.

Potyondy, D. (2012a) "*PFC2D* Flat-Joint Contact Model," Itasca Consulting Group, Inc., Minneapolis, MN, Technical Memorandum ICG7138-L, July 26, 2012.

Potyondy, D.O. (2012b) "A Flat-Jointed Bonded-Particle Material for Hard Rock," paper ARMA 12-501 in Proceedings of 46th U.S. Rock Mechanics/Geomechanics Symposium, Chicago, USA, 24–27 June 2012.